Paleoceanography and Paleoclimatology

RESEARCH ARTICLE
10.1029/2021PA004364

Cenozoic Proxy Constraints on Earth System Sensitivity to Greenhouse Gases

S. J. Ring[1,2], S. G. Mutz[1], and T. A. Ehlers[1]

[1]Department of Geoscience, University of Tübingen, Tübingen, Germany, [2]Section 3.3 Earth Surface Geochemistry, Deutsches GeoForschungsZentrum GFZ, Potsdam, Germany

Key Points:

- Large compilation of Cenozoic paleoclimate proxies was analyzed
- Paleogene and Neogene were dominated by Earth system sensitivity of 4°C but sensitivity must have increased in the Plio-Pleistocene
- High Earth system sensitivity stresses the importance of climate change mitigation over adaptation

Supporting Information:

Supporting Information may be found in the online version of this article.

Correspondence to:

T. A. Ehlers,
todd.ehlers@uni-tuebingen.de

Citation:

Ring, S. J., Mutz, S. G., & Ehlers, T. A. (2022). Cenozoic proxy constraints on Earth system sensitivity to greenhouse gases. *Paleoceanography and Paleoclimatology*, *37*, e2021PA004364. https://doi.org/10.1029/2021PA004364

Received 22 SEP 2021
Accepted 22 NOV 2022

Author Contributions:

Conceptualization: S. J. Ring
Formal analysis: S. J. Ring, S. G. Mutz
Funding acquisition: T. A. Ehlers
Supervision: S. G. Mutz, T. A. Ehlers
Writing – original draft: S. J. Ring, S. G. Mutz, T. A. Ehlers

Abstract The long-term extent of the Earth system response to anthropogenic interference remains uncertain. However, the geologic record offers insights into this problem as Earth has previously cycled between warm and cold intervals during the Phanerozoic. We present an updated compilation of surface temperature proxies for several key time intervals to reconstruct global temperature changes during the Cenozoic. Our data synthesis indicates that Earth's surface slowly cooled by ca. 9°C during the early Paleogene to late Neogene and that continent-scale ice sheets developed after global temperature dropped to less than 10°C above preindustrial conditions. Slow cooling contrasts with the steep decrease in combined radiative forcing from past CO_2 concentrations, solar luminosity, and ocean area, which was close to preindustrial levels even as Earth remained in a much warmer state. From this, we infer that the Earth system was less sensitive to greenhouse gas forcing for most of the Cenozoic and that sensitivity must have increased by at least a factor of 2 during the Plio-Pleistocene. Our results imply that slow feedbacks will raise global surface temperatures by more than 3°C in the coming millennia, even if anthropogenic forcing is stabilized at the present-day value (2 W/m^2), and that their impact will diminish with further warming.

Plain Language Summary It is not well known how much Earth's surface temperature will change over the next few millennia as a result of increasing atmospheric CO_2 concentrations. This is because we still have a limited understanding of many slow climate feedback mechanisms activated by climate change that will become important in the future. Most climate models project eventual global warming of 3–4°C for doubled CO_2 concentration but exclude many slow climate feedbacks, such as shrinking ice sheets. The distant (geologic) past provides additional clues about the future because the climate system and all of its feedbacks were in equilibrium with naturally elevated CO_2. Using up-to-date geologic information of the last 50 million years, we find that Earth's climate history is best described by a switch from a moderate sensitivity, close to that found in climate models, to a much higher sensitivity in the last 3 million years. If Earth behaves the same way today as it has done in the past, melting ice sheets, natural aerosols, and shifting vegetation patterns will slowly continue to raise global warming above the 2°C target during the next few thousand years even if the human contribution does not increase any further.

1. Introduction

Climate sensitivity is defined as the global surface temperature response (ΔGST) to a given radiative forcing (ΔF) and, as such, forms an important factor in predicting the evolution of the climate system during the Anthropocene. The surface temperature at which the planet achieves radiative equilibrium is set by the interaction of numerous components of the Earth system, such that the magnitude and behavior of climate sensitivity under various levels of forcing remain difficult to constrain (Knutti et al., 2017). The target quantity of interest in most studies using climate models and instrumental observations is called the equilibrium climate sensitivity (ECS). ECS only considers the behavior of climate feedbacks with a centennial response timescale, including those that amplify (e.g., water vapor, sea ice, and clouds) or attenuate temperature changes (e.g., lapse rate adjustment), and is therefore considered the best measure for the expected global-scale atmospheric response to human perturbation within the near future (e.g., Sherwood et al., 2020).

The geologic record is recognized as a powerful tool to elucidate the sensitivity of the climate system, as it contains numerous examples of a planet at steady state with elevated climate forcing created by changes in greenhouse gas concentrations, solar luminosity, and ocean area (Farnsworth et al., 2019; Rohling et al., 2012).

Knowledge of the temperature response across a wide range of boundary conditions can be used to refine the possible future climate trajectory during the Anthropocene (Rohling et al., 2012; Sherwood et al., 2020).

However, geologic climate proxies, by their very nature, provide an integrated picture of past climate states and record the behavior of all climate feedbacks regardless of their respective characteristic timescale or interactions. For example, full equilibration of the Earth system with elevated greenhouse gas concentrations will result in cryosphere retreat, a reduction in the planetary albedo, and therefore an amplification of the ΔGST response over what would be expected from ECS alone (Park & Royer, 2011; Royer, 2016; Wunderling et al., 2020; Zeebe, 2013). On the other hand, warming may lead to an expansion of global dryland area (Huang et al., 2015), which would elevate planetary albedo again due to intensified dust mobilization. In other words, many of the long-term processes, that make up Earth's climate system and are assumed to be constant in studies of ECS, are themselves controlled by the atmospheric carbon content as the governing Earth system parameter (Lacis et al., 2010). The fractional temperature response to both rapidly and slowly adjusting feedbacks is termed Earth system sensitivity (ESS) and represents the behavior of the climate system on a millennial timescale (Lunt et al., 2010).

Constraining ECS from paleoclimate data is only possible if independent estimates of all exogenic forcing factors and the magnitude of slow feedbacks in the past are available. For example, when paleoclimate models are forced with early Eocene boundary conditions (dimmer sun, vegetation distribution, continental configuration, and a lack of ice sheets) but preindustrial greenhouse gas concentration, simulated ΔGST tends to be around 5°C warmer than simulations of the present-day Earth (Caballero & Huber, 2013; Zhu et al., 2019). If this represents the effect of slow climate feedbacks which separate ESS from ECS, it can be used as a correction factor to calculate ECS from paleoclimate proxies (e.g., Anagnostou et al., 2016). Determining an equivalent correction factor for cooler parts of the Cenozoic is considerably more difficult since both volume and spatial distribution of planetary ice sheets are subject to substantial uncertainty. Indeed, the assumption of an ice-free world may not even be applicable for all parts of the Eocene (Carter et al., 2017; Gulick et al., 2017). Haywood et al. (2020) compared the simulated ΔGST of models organized within the Pliocene Model Intercomparison project (PlioMIP) with the ΔGST of the same models under idealized CO_2 doubling experiments. Since the Pliocene paleoclimate simulations prescribe many slow Earth system changes (approximating ESS), whereas CO_2 doubling experiments do not (approximating ECS), a normalization of ESS to ECS could isolate the impact of slow feedbacks. However, the role of Earth system changes in setting the steady-state Pliocene climate across PlioMIP models diverges by up to 250% (Haywood et al., 2020). This means that even for a closely studied and recent geologic period like the middle Pliocene, relative contributions of slow and fast feedbacks are poorly known.

This uncertainty is more severe for the Miocene and Oligocene, when estimates on the size of the cryosphere disagree by >50 m sea level-equivalent ice volume (Cramer et al., 2011; Lear et al., 2015; Marschalek et al., 2021; Wilson et al., 2013). Proxy-based constraints on ECS for much of the Cenozoic would therefore be highly dependent on an unknown ice-albedo correction, limiting their use in tracking the behavior of the climate system. Here, we instead restrict our analysis to a reconstruction of ESS by including known long-term radiative drivers of climate but avoiding corrections for slowly adjusting feedbacks. Observations show that these slow feedbacks are already active in the current climate system (e.g., Bjorkman et al., 2018; Willis et al., 2018) and are therefore expected to also play a role in future stages of the Anthropocene.

To estimate ESS, we rely on the large and growing proxy records of surface temperature and greenhouse gas concentration during the Cenozoic, which is by far the best sampled era of the Phanerozoic and most closely resembles the present-day Earth system. In Section 2, we present the details of our proxy compilation and our approaches to reconstructing the mean climate state through time. Section 3 provides a basic description of the results. These are finally discussed further in Section 4, in which we argue that the current proxy data support an abrupt twofold increase in ESS at some point of the Plio-Pleistocene.

2. Materials and Methods

2.1. Proxy Database Construction

We reconstruct the mean climate state of eight key time intervals across the Cenozoic, including the middle Pliocene (3.0–3.3 Ma), the late Miocene (7.2–11.6 Ma), the middle Miocene (14.7–17.0 Ma), the early Miocene (20.3–23.0 Ma), the early Oligocene (27.8–33.9 Ma), the late Eocene (33.9–37.8 Ma), the middle Eocene

(42.0–46.0 Ma), and the early Eocene (48.0–55.0 Ma). Many of these intervals have long been a research focus as they span the full range of paleoclimate conditions that have existed during the latest transition of the planet toward a global icehouse (Westerhold et al., 2020) and thus benefit from a comprehensive proxy coverage.

For each of these time intervals, we compiled globally distributed proxy estimates of land surface (LAT) and sea surface temperatures (SSTs) from previous studies. The proxies used in our analysis include paleofloral remains (e.g., leaf physiognomy, coexistence approach), inorganic sediment geochemistry (e.g., calcite Mg/Ca, clumped isotopes), lipid biomarkers (e.g., $U^{k'}_{37}$, TEX_{86}), and microfossil assemblages (e.g., diatoms). Whenever possible, raw proxy measurements were recalculated using the recent Bayesian calibration package for foraminiferal $\delta^{18}O$ (Malevich et al., 2019), foraminiferal Mg/Ca (Tierney et al., 2019), $U^{k'}_{37}$ (Tierney & Tingley, 2018), TEX_{86} (Tierney & Tingley, 2014), and MBT_{5me} (Crampton-Flood et al., 2020). The Bayesian calibration package calculates past surface temperature based on globally distributed core-top data. A table detailing the input parameters of each calibration model can be found in Supporting Information S1. Remaining proxy estimates, consisting mostly of paleobotanical and microfossil assemblages, were directly adopted from the primary literature.

Absolute proxy temperature estimates were converted to a corresponding temperature anomaly (ΔT) by first backtracking each site to its past coordinates using a model of global plate motion (Seton et al., 2012) and then subtracting the present-day (2008–2017) mean of the ERA5 reanalysis annual 2 m air temperature (for terrestrial proxies) or SST (for marine proxies) at the reconstructed paleo-location from the proxy-inferred temperature. Continental movement and draining of continental seas means that a few SST values are available for locations that are situated over land today. For those SST proxies, we used the mean annual SST of the nearest ERA5 ocean gridcell at the same paleo-latitude if the separation between the past location and the modern ocean is less than 3° of longitude, and the 2 m air temperature at the paleo-coordinates if the separation is larger than 3° of longitude.

Multiple data points for a single proxy are often available at one location (e.g., as part of a down-core time series of SST) or at locations that are within a tenth of a degree in latitude and longitude of each other. In both cases, we have taken the median value of all proxy data points within the relevant timeslice as the representative temperature value.

2.2. Calculation of ΔGST Anomaly

Previous studies describe multiple ways local ΔT values can be propagated from spatially disparate samples into a single ΔGST anomaly (Inglis et al., 2020). Here, we distinguish between three different zonal bins (90–60°N/S, 60–30°N/S, and 30°N–30°S paleolatitude) and average all temperature anomalies within these zones. A representative ΔGST for the time interval of interest is then determined by computing the sum of the average ΔT in each bin, weighted according to the respective fraction of global surface area covered by each bin. This method was first introduced by Caballero and Huber (2013) and has subsequently applied by others (e.g., Goldner et al., 2013; Inglis et al., 2020; O'Brien et al., 2020).

To assess the possible role of interproxy discrepancies within the database, we separately impose the following additional criteria: (a) exclusion of nonterrestrial proxies, (b) exclusion of nonmarine proxies, and (c) a combination case where we exclude data from orogenic regions as well as paleobotanical proxies from locations within tropical paleolatitudes (30°N–30°S).

A conservative Gaussian error of 5°C (95% interval) was assumed for each individual proxy estimate and combined with the standard deviation of proxy estimates within each zonal bin. Uncertainty was then propagated to the ΔGST estimate through random Monte Carlo subsampling ($n = 5{,}000$) of the data set and subsequent repetition of the same calculation. Out of the resulting distribution of ΔGST anomalies, we report the median value relative to the preindustrial period (1850–1899) as well as the 95% uncertainty envelope.

2.3. Calculation of Radiative Forcing

To investigate past ESS, the ΔF for each time period needs to be determined as well. One well-known forcing factor operating at multi-million-year timescales is a possible secular change in the mean atmospheric concentration of greenhouse gases, chiefly in the form of a declining CO_2 concentration. Just as for ΔT, there are numerous proposed ways to extract the ancient atmospheric composition from geologic proxies predating the ice core record. We therefore separate the CO_2 record into (a) stomatal physiognomy (taken from https://paleo-co2.org/),

(b) phytoplankton $\delta^{13}C$ (Rae et al., 2021; Witkowski et al., 2018), (c) calcite $\delta^{11}B$ (Anagnostou et al., 2020; Greenop et al., 2019; Sosdian et al., 2018), and (d) a combined average of marine proxies that incorporates both phytoplankton $\delta^{13}C$ and calcite $\delta^{11}B$. The average proxy CO_2 concentration within each study interval is converted to a corresponding radiative forcing using a radiative transfer function (Myhre et al., 1998):

$$\Delta F_{CO_2} = 5.35 \ln\left(\frac{C}{C_0}\right),$$

where C_0 is the preindustrial CO_2 concentration of 286 ppm. A combined error of the mean interval CO_2 concentration estimate is calculated by random Monte Carlo subsampling ($n = 5{,}000$) of each individual CO_2 data point within their respective uncertainty distribution and subsequent averaging between data points.

A second forcing factor is solar luminosity, which undergoes a well-defined gradual brightening, so the past radiative forcing can be calculated through the increase in solar irradiance (Gough, 1981):

$$\Delta F_{SOL} = \frac{(S_t - S_0)(1 - A)}{4},$$

$$S_t = \frac{1}{1 + \frac{2}{5}\left(1 - \frac{4700 - t}{4700}\right)} S_0,$$

where S_0 is the present solar constant (1,368 W/m^2), A is the planetary albedo (assumed to be equal to 0.29), and t is the age of a given point in time for which ΔF_{SOL} is to be calculated.

Lastly, we also try to correct for changes in surface albedo due to past continental movement that are independent of the climate state. Farnsworth et al. (2019) found that paleogeographic forcing is dominated by the fraction of Earth's surface covered by ocean. A change in ocean area will perturb the global radiative balance on account of the lower albedo of oceans compared to land. An approximation of the geographic forcing can therefore be made using reconstructions of the past ocean area (Farnsworth et al., 2019):

$$\Delta F_{GEOG} = \frac{0.08\,\Delta A S_0}{4},$$

where 0.08 is the albedo difference between continents and oceans and ΔA is the difference in ocean area compared to the present-day continental configuration.

2.4. Calculation of ESS From Paleo-Data

Comparison of the ΔGST record with proxy-based ΔF allows for a new quantification of climate sensitivity that is independent of sensitivity estimates based on climate models or observations of the present-day climate system. ESS was calculated by evaluating the linear regression of ΔGST against ΔF, where the regression gradient quantifies the sensitivity parameter (in °C/W/m^2), that is, the fractional change in ΔGST for a given change in imposed forcing. Due to convention, we also report the climate sensitivity as the temperature response to doubled carbon dioxide (in °C), which can be assessed by multiplying the sensitivity parameter with an associated forcing of 3.7 W/m^2 (Myhre et al., 1998).

3. Results

3.1. Zonal and Global Mean Temperature

Our data compilation reveals a consistent pattern of past polar amplification, with large temperature changes near the poles and modest changes in the tropics (Figures 1 and 2). The highest ΔT values during any timeslice are consistently found above 60° in paleolatitude and at times exceed 30°C ΔT (relative to the present-day; Figure 1). On the other hand, calculated tropical surface temperature anomalies are within a ΔT of 15°C, even during the warmest prolonged periods of the Cenozoic. Indeed, the tropical ΔT of most periods is hard to distinguish from modern conditions as proxies seldom record anomalies of more than 5°C and include many sites with apparent past temperatures that are somewhat cooler than today (Figures 1 and 2).

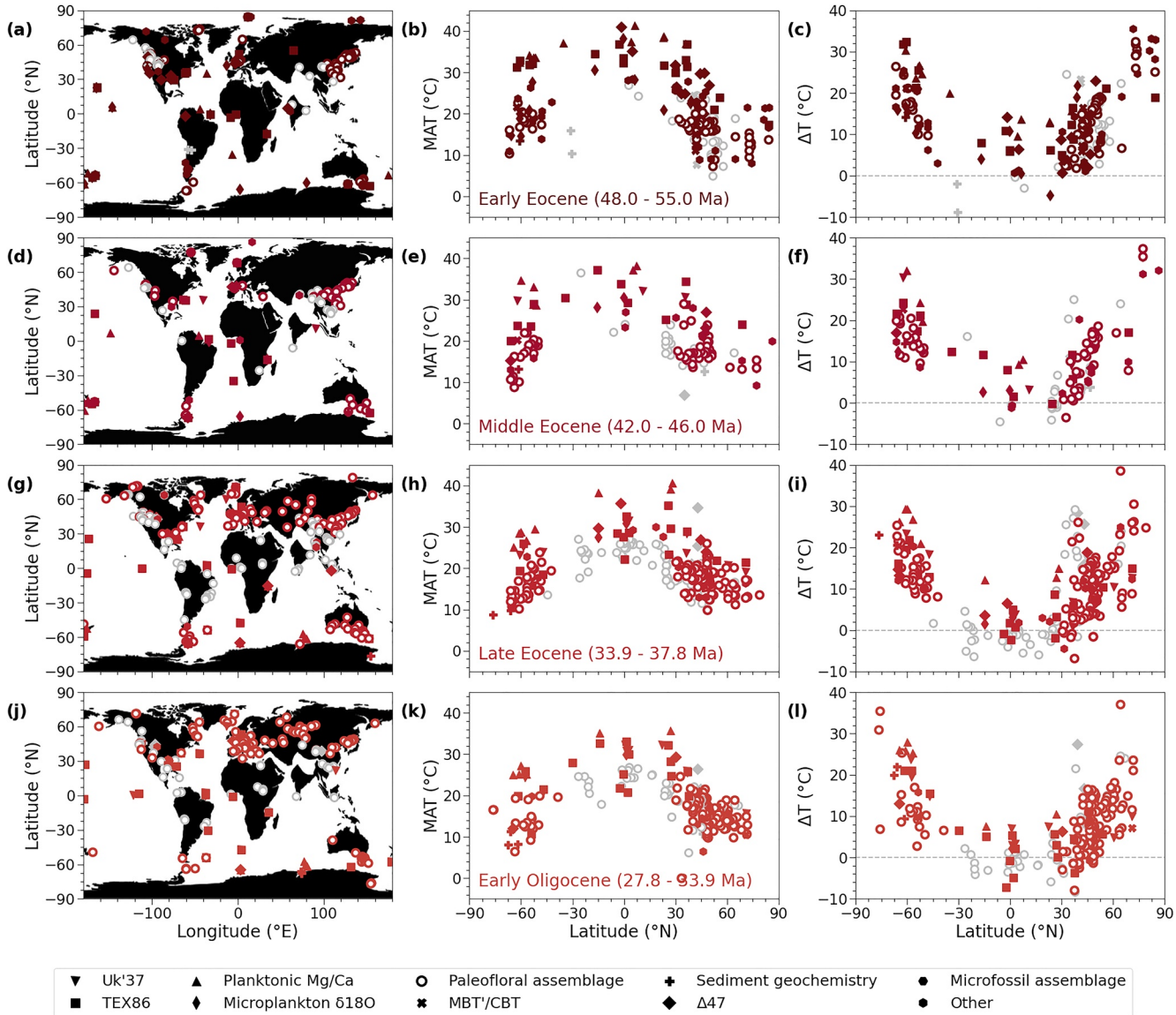

Figure 1. Paleogeographic distribution and calculated temperature anomalies of proxy records within the selected Paleogene study intervals. The compilation includes data for the early Eocene (a–c), the middle Eocene (d–f), the late Eocene (g–i), and the early Oligocene (j–l). ΔT is the difference between the present-day (2008–2017) mean annual surface temperature at the backtracked geographic position of each proxy record and the proxy-inferred temperature. Data points that we later exclude in our preferred ΔGST calculation are shown in gray.

Amplified polar ΔT changes are a uniform feature of our proxy compilation but zonal temperature histories nevertheless differ between both hemispheres (Table 1), particularly in polar regions. Averaged proxy results from the Arctic suggest steep cooling from the early Eocene to the early Oligocene, followed by stable temperate conditions that lasted into the Pliocene (Figure 3a). Temperatures in the Antarctic coastal regions were, on average, more invariant until the early Oligocene and began to cool throughout the Neogene toward the present (Figure 3b). This leads to large hemispheric differences in ΔT of up to 8°C (Figure 3c). Proxy estimates from middle and low latitudes are, in contrast, in better agreement and differ by 5°C in some parts of the Paleogene and 3°C or less during the remaining Cenozoic.

Large differences in the inferred ΔT and ΔGST are also observed when separating the data between proxies with either a marine or terrestrial provenance, the latter of which are dominated by paleobotanical temperature estimates. Terrestrial proxies suggest extreme warming at high latitudes in both hemispheres and are in close agreement with marine proxy estimates (Figures 3d and 3e). At the same time, they clearly fall below marine

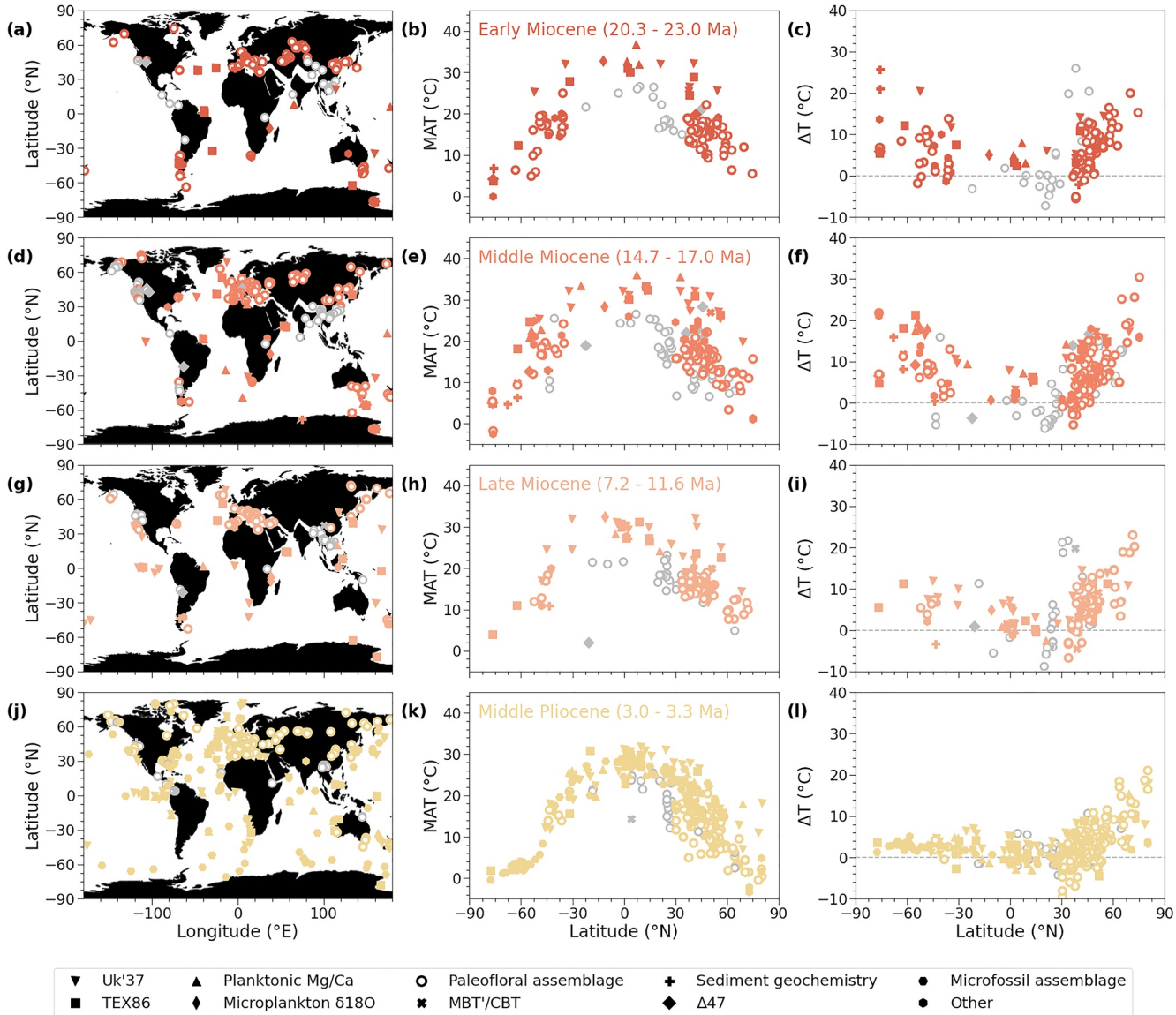

Figure 2. Paleogeographic distribution and calculated temperature anomalies of proxy records within the selected Neogene study intervals. The compilation includes data for the early Miocene (a–c), the middle Miocene (d–f), the late Miocene (g–i), and the middle Pliocene (j–l). ΔT is the difference between the present-day (2008–2017) mean annual surface temperature at the backtracked geographic position of each proxy record and the proxy-inferred temperature. Data points that we later exclude in our preferred ΔGST calculation are shown in gray.

proxies in extrapolar latitudes of every timeslice, where the mean zonal SST is often around 4°C warmer than LAT (Figure 3f). Marine proxies, for instance, are uniform in supporting a modestly warmer tropical ocean during the entire Cenozoic, whereas warmer-than-present conditions for tropical land surfaces are only apparent for the early Eocene. Latitudes between 60°N and 60°S together comprise about 87% of Earth's surface, so discrepancies in SST and LAT in those regions yield similar discrepancies in globally averaged values, which are around 3°C warmer when using marine over terrestrial proxies (Table 1).

In addition, terrestrial proxies do not resolve the same temperature trends as marine proxies through time. Average SSTs in every zonal bin show warming from the early to middle Miocene (Figure 3e). A similar transient warming is not apparent in LAT, which instead suggests uninterrupted cooling during the Miocene and throughout the Cenozoic as a whole. The early Neogene (ca. 16 million years ago) thus stands out as a uniquely uncertain time period, when the discrepancy between SST and LAT peaks at around 7°C outside of polar regions (Figure 3f), translating to a ΔGST difference of 6°C.

Table 1
Overview of Interval-Averaged Zonal and Global Mean Temperature Anomalies Under Different Treatments of the Multiproxy Database

		Middle Pliocene	Late Miocene	Middle Miocene	Early Miocene	Early Oligocene	Late Eocene	Middle Eocene	Early Eocene
Multiproxy (entire data set)	High lat.[a] ΔT (°C)	9.0	12.3	14.2	12.1	17.6	19.3	21.3	24.7
	Midlat.[b] ΔT (°C)	2.5	6.3	7.1	6.7	7.7	11.3	11.6	12.0
	Low lat.[c] ΔT (°C)	0.9	1.0	0.1	0.9	0.9	0.8	2.7	5.6
	ΔGST (°C)	3.5	5.4	5.5	5.5	6.6	8.1	9.4	11.4
SST only (excluding proxies from continents)	High lat. ΔT (°C)	7.4	9.3	11.8	7.9	18.4	18.5	21.3	22.3
	Midlat. ΔT (°C)	3.3	8.5	13.7	7.6	11.2	13.2	12.8	15.9
	Low lat. ΔT (°C)	1.6	2.4	5.1	4.6	3.1	4.4	5.0	6.9
	ΔGST (°C)	3.9	6.5	10.1	7.1	9.1	10.4	11.0	13.2
LAT only (excluding proxies from oceans)	High lat. ΔT (°C)	9.3	13.2	14.6	13.2	17.4	19.6	21.4	25.5
	Midlat. ΔT (°C)	2.2	5.9	6.1	6.6	7.4	11.1	11.2	11.3
	Low lat. ΔT (°C)	0.2	−0.5	−2.0	−1.0	−0.4	−0.6	1.1	3.1
	ΔGST (°C)	3.1	4.6	4.1	4.6	5.7	7.3	8.4	10.0
Combination (excluding proxies from orogenic belts and botanical data from paleotropics)	High lat. ΔT (°C)	9.0	12.7	15.1	12.1	17.2	19.1	21.2	24.8
	Midlat. ΔT (°C)	2.5	5.8	7.3	6.2	7.4	10.5	11.7	13.1
	Low lat. ΔT (°C)	1.8	2.4	5.1	4.6	3.1	4.4	5.0	6.9
	ΔGST (°C)	3.9	5.9	8.2	7.1	7.5	9.5	10.5	12.5

[a]90°N/S–60°N/S. [b]60°N/S–30°N/S. [c]30°N–30°S.

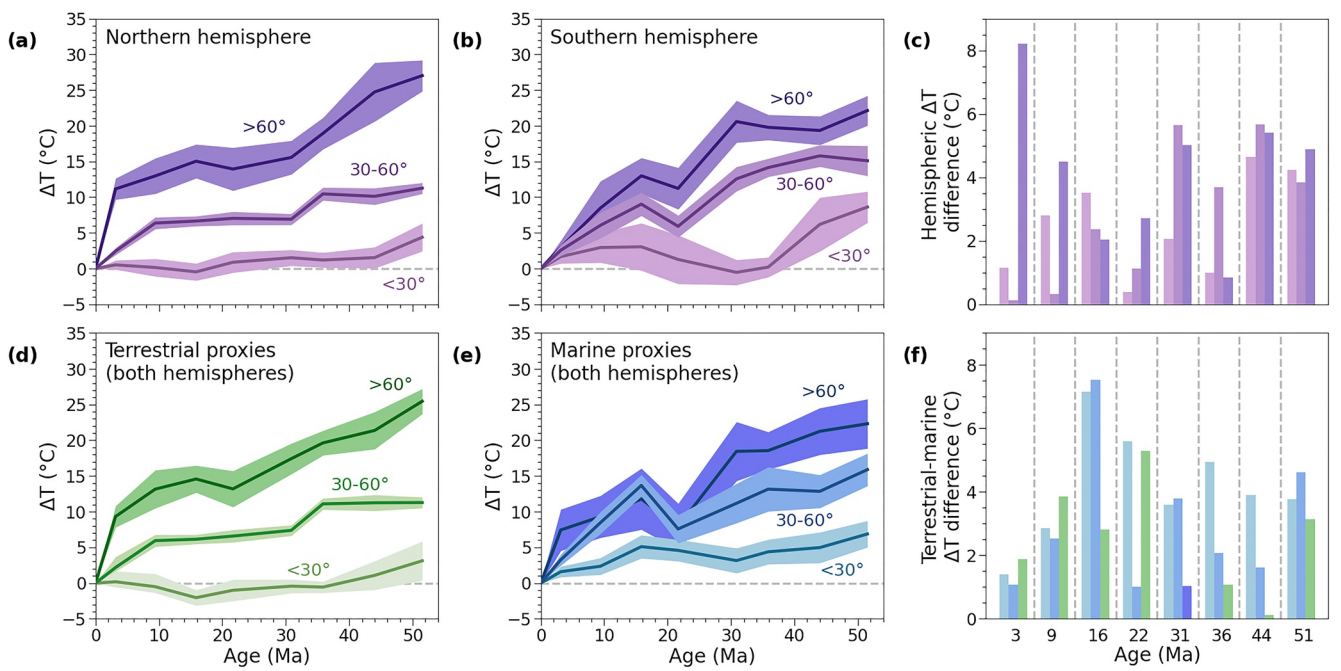

Figure 3. Average zonal temperature change of the three zonal bins (high latitudes, middle latitudes, low latitudes) that are used to calculate ΔGST, relative to the present-day. High latitudes are indicated by the darkest color and low latitudes by the brightest. Multiproxy zonal averages of ΔT in the Northern Hemisphere (a) and Southern Hemisphere (b) indicate the same general cooling but show some distinct differences (c). Similarly, terrestrial proxies (d) and marine proxies (e) in both hemispheres often differ by around 3°C and up to 8°C in the middle Miocene (f). These differences are most likely a product of differences in sample coverage and systematic biases of some proxies (see main text). Note that panels (a) and (b) show raw multiproxy averages without additional corrections.

Table 2
Overview of Interval-Averaged Atmospheric CO_2 Estimates and Associated Radiative Forcing

		Middle Pliocene	Late Miocene	Middle Miocene	Early Miocene	Early Oligocene	Late Eocene	Middle Eocene	Early Eocene
Stomata	Median CO_2 (ppm)	358	384	492	571	491	496	733	591
	Median ΔF_{CO2} (W/m^2)	1.20	1.58	2.90	3.70	2.70	2.95	5.04	3.89
Phytoplankton $\delta^{13}C$	Median CO_2 (ppm)	256	373	482	701	655	638	748	1,122
	Median ΔF_{CO2} (W/m^2)	−0.60	1.42	2.79	4.79	4.43	4.30	5.14	7.31
Calcite $\delta^{11}B$	Median CO_2 (ppm)	408	392	492	309	842	893	984	1,185
	Median ΔF_{CO2} (W/m^2)	1.90	1.69	2.90	0.42	5.78	6.09	6.61	7.61
Phytoplankton $\delta^{13}C$ + calcite $\delta^{11}B$ (preferred)	Median CO_2 (ppm)	362	371	489	374	671	742	995	1,172
	Median ΔF_{CO2} (W/m^2)	1.25	1.40	2.87	1.44	4.56	5.10	6.67	7.54
Solar luminosity	ΔF_{SOL} (W/m^2)	−0.06	−0.21	−0.31	−0.44	−0.66	−0.72	−0.91	−1.03
Paleogeography	ΔF_{GEOG} (W/m^2)	+0.03	+0.05	+0.08	+0.11	+0.16	+0.19	+0.49	+0.44

Regardless of proxy choice, ΔGST results indicate a large-magnitude global cooling of at least 7°C from the Eocene to the Pliocene. In addition, proxies suggest that global cooling was sufficiently slow for Earth's climate system to remain in a much warmer state of at least 4°C ΔGST for the majority of the Cenozoic.

3.2. Atmospheric CO_2 and Radiative Forcing

Time-averaged values of atmospheric CO_2 by different paleobarometers are provided in Table 2. The different proxies are in good agreement in suggesting moderately elevated CO_2 concentrations during the middle Pliocene, late Miocene, and middle Miocene but they produce different results for the earlier time periods. In general, all three proxies support a long-term decline of atmospheric CO_2 in the sense that the highest values are found in the earliest timeslices. They however differ in the apparent pacing of CO_2 reduction. For the Paleogene, stomatal parameters suggest moderate CO_2 concentrations of between 500 and 600 ppm while phytoplankton $\delta^{13}C$ and calcite $\delta^{11}B$ suggest one to two halvings of the CO_2 concentrations from peak values of more than 1,100 ppm as determined for the early Eocene.

Overall, CO_2 proxies indicate a drop in greenhouse gas radiative forcing (ΔF_{CO2}) of 5–8 W/m^2 from the early Eocene to the present (Table 2). This trend has been partially compensated by the combined effects of increasing solar brightness (ΔF_{SOL}) and a reduction in the global ocean surface area (ΔF_{GEOG}) that collectively contribute an increase of 0.6 W/m^2 (Table 2).

3.3. Earth System Sensitivity

Figure 4 shows the results of our forcing estimates from selected CO_2 proxies against uncorrected multiproxy ΔGST values. Equivalent figures for alternative ΔGST estimates and tabulated ESS results associated with every proxy combination can be found in Supporting Information S1. Despite the variability and uncertainty of the proxy estimates outlined above, inferred values for ESS for various combinations of temperature proxies and CO_2 paleobarometers only span a relatively narrow range of 0.8–1.3°C/W/m^2, or 3.0°C–4.7°C for every doubling in CO_2 concentrations. In our approach, ESS is the average collective slope of all Cenozoic timeslices rather than the point-wise collection of slopes between individual timeslices and the preindustrial (i.e., the origin of the ΔF–ΔGST crossplot). In other words, the ESS estimate is derived from the relative climate evolution between our timeslices rather than the position of each timeslice compared to the preindustrial. For example, adopting marine or terrestrial proxies in the ΔGST estimate instead of the multiproxy average merely shifts all timeslices to higher or lower temperatures (respectively) by comparable amounts and hence does little to change the slope between them.

The choice of which proxy is used nevertheless does have a marked influence on the apparent coherence of the ΔF–ΔGST relationship. In general, using marine ΔT and stomatal CO_2 estimates results in the highest ESS and

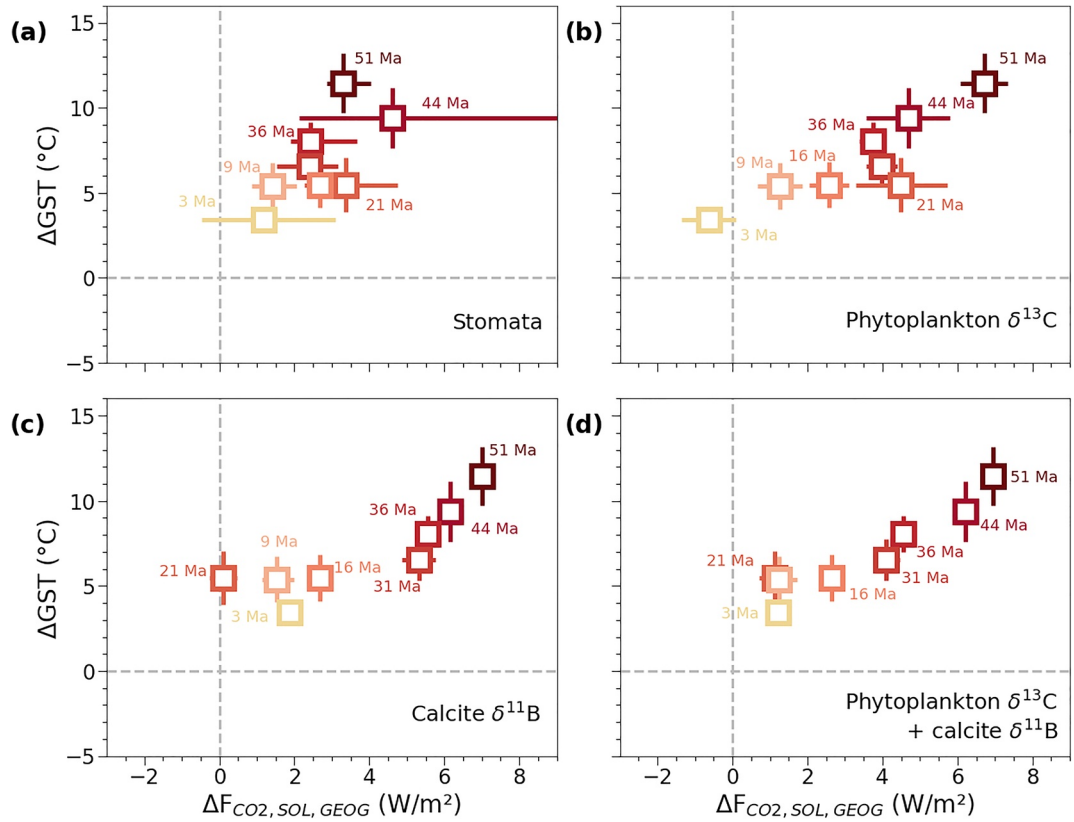

Figure 4. Scatterplots of median ΔF and ΔGST results of each Cenozoic timeslice. The data shown in this figure are based on the multiproxy ΔGST (Table 1) and compared to forcing estimates based on atmospheric CO_2 estimates from stomatal physiognomy (a), phytoplankton $\delta^{13}C$ (b), calcite $\delta^{11}B$ (c), and an average of phytoplankton $\delta^{13}C$ and calcite $\delta^{11}B$ (d). See Supporting Information S1 for equivalent plots using alternative ΔGST estimates.

the largest residual scattering of timeslices ($r^2 \approx 0.5$). Marine CO_2 proxies tend to yield a more well-defined relationship ($r^2 > 0.6$) but at somewhat lower ESS (see Supporting Information S1).

We also applied an ANOVA test for possible nonlinear behavior within our data set, such as an increasing slope (and thus increasing ESS) in warmer climate states. The ANOVA test evaluates whether a quadratic model provides a closer fit to our results than a linear one, where high p values denote a high probability for a linear relationship. We find that most proxy combinations are satisfactorily described by a linear fit (ANOVA $p > 0.05$; see Supporting Information S1). A second-order polynomial only appears to provide an improved fit compared to a linear one (ANOVA $p < 0.05$) in two instances where the greenhouse gas forcing is based on data from calcite $\delta^{11}B$ (as is this case in Figure 4c). We thus assume a linear slope with constant ESS between timeslices for the remaining text.

4. Discussion

4.1. Determining a Best Estimate of ΔGST and ΔF

Surface cooling and CO_2 decrease appear as robust features of the Cenozoic paleoclimate record but proxies clearly disagree on the magnitude of these processes. To gain an accurate understanding of how Earth's climate system evolved through time, we first provide an interpretation for the best estimates of ΔF and ΔGST. These estimates are then discussed in further detail in the following sections.

One important development during the Cenozoic is the tectonic uplift of several major orogenic plateaus (Barnes & Ehlers, 2009; Botsyun et al., 2019) and some of the highest terrestrial proxy-based ΔT in many time periods are sourced from locations at high modern altitude (e.g., Fan et al., 2014; Page et al., 2019). Temperature proxies within orogenic belts that may have been situated at lower elevation during the time of their deposition would

exhibit artificially high ancient ΔT since the difference between past and present temperature would be dominated by cooling related to uplift as opposed to global climate change. ΔGST for any time period would thus be biased toward high values if a considerable fraction of data are located in tectonically active regions.

A second possible source of bias are the muted temperature changes we observe on continents, which were about 4°C cooler in zonal average ΔT (Figure 3f) and up to 10°C cooler within some regions compared to the ocean surfaces (Figure 1c). Previous compilations have noted an equivalent discrepancy between marine and terrestrial proxies (e.g., Burls et al., 2021). Our results demonstrate that this is in fact a pervasive phenomenon of paleoclimate data between the early Eocene and Pliocene. Larger temperature changes determined for the surface ocean conflict with the physical expectation that warming should be amplified over land (Byrne & O'Gorman, 2018; Sutton et al., 2007). This indicates the presence of an unrecognized temperature bias. One common explanation is that the primary production of geochemical indices that are used to reconstruct SST could be larger during the warm summer season, shifting the measured signal toward temperatures higher than the annual average (Davies et al., 2019). This mechanism is often invoked to explain proxy results in polar regions (e.g., Bijl et al., 2013; Contreras et al., 2014). However, a summer bias in marine proxies alone is not sufficient to explain our observations. The difference between terrestrial and marine realms is in fact greatest in the middle and low latitudes (Figure 3f), where the seasonal contrast is reduced or even absent.

Most terrestrial proxies are based on the physiognomy of fossil plants and rely on the temperature tolerance ranges of nearest living relatives to extinct taxa (e.g., Utescher et al., 2014), that is, past LAT is reconstructed from a fossil assemblage by the shared overlap of temperature ranges of the closest extant analogue species. Reliable temperature reconstructions are only possible provided climatic niches of taxonomic lineages are conserved through time. Botanical assemblages are thus ill-suited for the reconstruction of tropical surface conditions because extinct organisms in those regions likely existed in annual surface temperatures higher than any found on Earth today (~30°C) and detection of surface temperatures outside the calibration range cannot be made through taxonomic analogs. Indeed, some workers have pointed to broader structural flaws in the most common paleobotanical approach to question the reliability of temperature reconstructions in general (Grimm & Potts, 2016; Grimm et al., 2016). In any case, cooler-than-present ΔT determined for tropical regions of many time periods (Figures 1 and 2) most likely reflects a methodological limitation at high temperatures that leads to an underestimation of past warming.

Based on the discussion above, we suggest the most parsimonious way to treat the multiproxy ΔT compilation is to accept all proxy results within the data set except for any data from orogenic plateaus, as well as floral assemblage from low paleolatitudes (30°N–30°S). We refer to this selection of reliable proxy results as "combination" (Table 1). This approach removes the most biased proxy results while also remaining agnostic about the accuracy of geochemical versus floral proxies outside the tropics and preserving the widest possible proxy diversity.

Equally, proxies of the atmospheric CO_2 concentration suffer from unique shortcomings that limit their use in paleoclimate studies. For example, stomatal density and leaf conductance which underpin paleobotanical estimates of CO_2 can also vary as a function of ambient temperature and humidity (Konrad et al., 2020). Carbon isotopic fractionation during photosynthesis in marine phytoplankton is similarly dependent on a suite of physiological influences that are poorly constrained for the past (Zhang et al., 2020). Boron isotopes finally require independent measurements or assumptions on the secular changes in seawater $\delta^{11}B$ as well as other parts of the ocean carbonate system (Foster & Rae, 2016; Rae et al., 2021). With these caveats in mind, we use the average of both phytoplankton $\delta^{13}C$ and calcite $\delta^{11}B$ as our preferred way to derive past greenhouse gas forcing (Table 2). These methods have the most direct physicochemical connection to the marine carbon cycle (Rae et al., 2021) and thus hold great promise in a quantitative reconstruction of ancient CO_2 concentrations.

4.2. Patterns of Cenozoic Temperature Change

Long-term global cooling from the early Eocene to the Pliocene is evident from the advance of glacial deposits (Macdonald et al., 2019; Figure 5a) and the 4‰ enrichment of oxygen isotopes in benthic calcareous microplankton (Westerhold et al., 2020; Figure 5b). Our preferred proxy choice (excluding low-latitude plant assemblages and data from orogenic belts) indicates that Earth's surface underwent a large-magnitude global cooling of 9°C in the same time period, in a two-step fashion that matches the oxygen isotope record (Figure 5c).

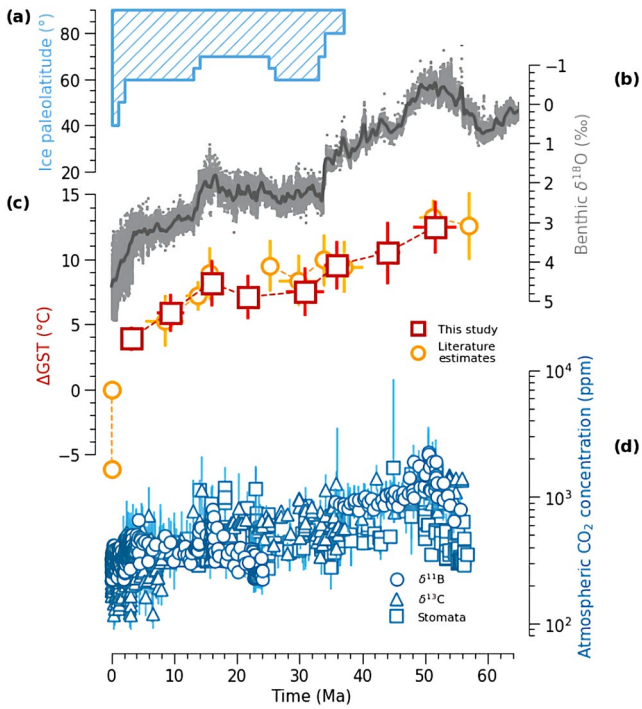

Figure 5. Composite climate evolution over the last 50 million years. Global cooling is clearly indicated by the latitudinal extent of glacial deposits (Macdonald et al., 2019) (a) and the increasingly heavier benthic foraminiferal $\delta^{18}O$ (Westerhold et al., 2020) (b). (c) The spatially weighted proxy synthesis (red; this study) indicates progressive surface cooling of ca. 9°C, which was accompanied by approximately two halvings in atmospheric CO_2 concentration (d). A few selected literature ΔGST estimates (orange; Burls et al., 2021; Inglis et al., 2020; O'Brien et al., 2020; Tierney et al., 2020) have also been added for comparison.

Highest sustained ΔGST of 12.5°C (±2.0°C, 95% interval) are found during the early Eocene (Figure 5c), in close agreement with the results of Inglis et al. (2020). Climate states of the middle Eocene (10.5°C ± 2.4°C ΔGST, 95% interval) and late Eocene (9.5°C ± 1.8°C ΔGST, 95% interval) are above the proxy-constrained simulations of Cramwinckel et al. (2018) but are bracketed by those of Baatsen et al. (2020). In general, the range of Eocene ΔGST supports the notion that Earth lacked a substantial cryosphere for most of the Eocene, as ice sheet models suggest a ΔGST of 10°C as the threshold value for deglaciation of Antarctica (Garbe et al., 2020).

We also find evidence for a warm, equable greenhouse climate during the early Oligocene (7.5°C ± 1.9°C ΔGST, 95% interval), implying a moderate temperature drop compared to the preceding Eocene. The Eocene–Oligocene boundary is traditionally viewed as the onset of continent-scale glaciation in Antarctica, with glaciers capable of intermittently reaching sea level (Liebrand et al., 2017). Climate model simulations suggest that the emplacement of a large Antarctic ice sheet on its own is associated with significant steering of atmospheric and oceanic circulation that induces a warming response over much of Earth's surface (Goldner et al., 2013; Kennedy et al., 2015). This may account for the modest cooling observed for most proxies across the Eocene–Oligocene. However, the question remains how a voluminous ice sheet was able to form and be sustained in a much warmer climate state like the Oligocene in the first place (O'Brien et al., 2020). In fact, we are able to extend this paradox to much of the subsequent Neogene. Sedimentological indicators for large ice sheets in a meltwater-rich subpolar Antarctic environment (Fielding, 2018; Gulick et al., 2017; Levy et al., 2016; Marschalek et al., 2021) coincide with heightened ΔGST. For example, Lear et al. (2015) argued on the basis of coupled Mg/Ca-$\delta^{18}O$ measurements of benthic foraminifera that global ice volume exceeded that of the present-day for much of the Neogene and reached a maximum during the late Tortonian, a time for which we obtain a ΔGST of 5.9°C (±1.4°C, 95% interval). Further corroboration would hint at the controlling influence of factors that are independent of the global climate, such as paleotopography (Paxman et al., 2020), on the equilibrium ice volume in Antarctica.

Although the Cenozoic is punctuated by rapid carbon release events with attendant changes in the Earth system (Turner et al., 2014), overall cooling of the mean background climate proceeded at a rate of little over 0.1°C per million years. Interestingly, an emerging body of evidence suggests that glacial periods of the late Pleistocene were marked by ΔGST as low as −6°C (Snyder, 2016; Tierney et al., 2020), just 2 million years after our youngest timeslice (Figure 5c). Glacial climates clearly form the cold end of large temperature oscillations that dominated the last 1 million years but even a time-averaged ΔGST of −3.5°C (Snyder, 2016) is incompatible with the slow rate of cooling observed for the Paleogene and Neogene. Cold conditions of the late Pleistocene thus imply an acceleration of the long-term rate at which Earth cooled by 1 order of magnitude (approximately 2.7°C per million years).

The gradual emergence of a colder climate state is also apparent from high-latitude biomes and their transition over the Cenozoic. Eocene sedimentary deposits suggest the presence of evergreen rainforests around the Ross Sea (Pross et al., 2012) and on several Arctic islands (Suan et al., 2017; West et al., 2015). By the early to middle Miocene, polar warmth had restricted Antarctic vegetation to prostrate shrublands on the coast (Warny et al., 2009) and fragmented tundra terrains in the continental interior (Lewis et al., 2008). Terrestrial palynomorphs are finally absent during the Pliocene (Anderson et al., 2011), indicating the local extinction of most vascular plants on Antarctica at some point in the late Miocene.

Considering our preferred proxy treatment (Table 1), polar ΔT changes were on average 4.3 (±2.1, 95% interval) times larger than tropical ΔT and 2.0 (±0.4, 95% interval) times larger than ΔGST. Proposed mechanisms governing the meridional temperature structure in the past, such as biologically induced cloudiness (Kump &

Pollard, 2008), invigorated ocean heat transfer (Batenburg et al., 2018), or water vapor buoyancy (Seidel & Yang, 2020) remain enigmatic and continue to be debated. Unfortunately, our ΔT compilation alone is not diagnostic in this regard because many different processes could produce identical temperature patterns.

There are also some indications that polar amplification may not be homogeneous across both hemispheres. During several Cenozoic timeslices, apparent high-latitude warming of the Arctic exceeds that of the Antarctic by more than 4°C (Figure 3c). Zonal bins in our analysis are coarse, covering 30° in latitude. Hemispheric differences in ΔT can arise if those zones are not sampled equally well. This is a particular problem for high latitudes, where ice sheets have stripped away large volumes of continental sediment or drape existing fossil sites. For example, our middle Eocene compilation features numerous ΔT estimates that originate close to the paleo-North pole (up to 86°N) but the most southerly data point only extends to 66°S (Figures 1a–1c). Since the most pronounced ΔT changes will presumably be found near the pole, middle Eocene southern high-latitude warming could be underestimated. This may account for most of the hemispheric asymmetry at this time.

On the other hand, the same sampling artifacts cannot explain the hemispheric difference during the middle Pliocene, which has a similar poleward coverage (80°N–78°S; Figures 2j–2l). Large warming of around 15°C across the Pliocene Arctic is indicated by a wide array of different climate proxies (Ballantyne et al., 2010; Figure 2l) and allowed for the maintenance of cool deciduous and mixed coniferous forests. A similarly amplified response is not seen in austral high latitudes (Figure 2l). One site that is well situated to ascertain whether this is a genuine phenomenon are the Oliver Bluffs in the Transantarctic mountains (85°S). Here, mummified leaves of southern beech (*Nothofagus*) point to mean annual temperatures of around −12°C, about 14°C warmer than at present-day (Francis & Hill, 1996) and well in line with middle Pliocene ΔT of the Northern Hemisphere. Unfortunately, the age of the Oliver Bluffs strata are uncertain and have been variously dated to between 3 and 17 million years (Barrett, 2013) and therefore could not be included in our data set. The reasons why near-modern temperatures may have been maintained in the Pliocene Southern Ocean are also unclear. Some PlioMIP models suggest significant hemispheric differences in warming, but these are not coherent throughout the ensemble and the multimodel mean hence supports a symmetrical ΔT pattern with a warm Southern Ocean (Haywood et al., 2020). At present, only one ΔT data point in this region is derived from a geochemical proxy (McKay et al., 2012) while all others are based on diatom assemblage transfer functions. Future investigations may determine larger Pliocene warmth on the Antarctic perimeter but cool conditions remain an enigmatic feature in the current proxy record.

4.3. Deep Ocean ΔT_D and Cretaceous ΔGST

When we pair ΔGST with estimates of average concomitant deep ocean temperatures (ΔT_D) for each of our timeslices (Cramer et al., 2011; mean value of their equations 7a and 7b), results suggest a close dependence ($r^2 = 0.8$) at a rate of 1.0°C (±0.2°C, 95% interval) change in ΔGST for every 1°C change in ΔT_D. This supports previous findings of a direct correspondence between the global surface and the deep ocean (Krissansen-Totton & Catling, 2017). If the same relationship also holds for the younger periods of the Mesozoic, extreme deep ocean warming during the Cenomanian-Turonian Thermal Maximum (Cramer et al., 2011) predicts a middle Cretaceous ΔGST of close to 20°C—consistent with coeval elevated SSTs (O'Brien et al., 2017) and atmospheric CO_2 concentration (Witkowski et al., 2018). Combined with ΔGST data of the late Cenozoic (Snyder, 2016), a hot middle Cretaceous implies that Phanerozoic transitions from ice-free hothouse to heavily glaciated icehouse states may cover a ΔGST range of up to 26°C.

A one-to-one correspondence between ΔGST and ΔT_D is however surprising in light of the supposed bottom water source region. Saline bottom water bathing the ocean floor is thought to have been generated around the Antarctic shelf throughout the Cenozoic (Hollis et al., 2012; Huck et al., 2017). Since temperature changes appear to be amplified at high latitudes (Figures 1–3), ΔT_D is expected to match the ΔT evolution indicated by polar proxies rather than the global average ΔGST. One way to reconcile proxies from the polar surface with those at depth is to presume that these archives are biased toward opposite seasons of the annual cycle. Surface proxies could be biased toward the polar summer (see Section 4.1) while models suggest that formation of deep water is strongest in winter (Baatsen et al., 2020; Hollis et al., 2012).

Another complication is that the ΔT_D used here is based on the calcite Mg/Ca of benthic foraminifera which has multiple additional controls besides ambient temperature. The sensitivity of shell Mg/Ca to the secular drift in the Mg/Ca of seawater is a debated uncertainty of this proxy (de Nooijer et al., 2017; Evans et al., 2015) and could

lead to an underestimation of ΔT_D. An alternative archive to estimate ΔT_D is clumped isotope paleothermometry of benthic foraminifera, which is independent of seawater chemistry. Clumped isotope data (e.g., Modestou et al., 2021) indeed often yield ΔT_D values that are in excess of the compilation by Cramer et al. (2011). The spatial and temporal paucity of these samples, however, means that clumped isotopes cannot yet provide firm insight into long-term ΔT_D changes spanning the Cenozoic, though the first long-term compilation has recently become available (Meckler et al., 2022).

4.4. Proxy Constraints on ESS

Cenozoic timeslices represent a succession of different paleoclimate states. Matching our preferred estimate ranges for ΔGST with coeval changes in the radiative forcing that supported each time period allows for improved quantification of ESS (equivalent to $S_{[CO2,SOL,GEOG]}$ in Paleosens notation; Rohling et al., 2012). The combined effects of variations in atmospheric CO_2 concentration, solar brightening, and changing ocean area lead to a substantial reduction in the surface radiative balance of 7 W/m^2 (Table 2). Evolution of associated ΔGST is more subdued as Earth appears to have remained in a hot or mild greenhouse state throughout all timeslices, even at times when ΔF approached near-preindustrial levels in the Neogene (Figure 4).

Results from an ordinary least squares regression yield a best estimate ESS of 1.1°C/W/m^2 (±0.3°C/W/m^2, 95% interval) or 3.9°C (±1.1°C, 95% interval) for every doubling of CO_2 concentration. This magnitude is in agreement with several studies (Knobbe & Schaller, 2018; Martínez-Botí et al., 2015; Wong et al., 2021) but low compared to most of the literature which favors an ESS of 5°C or more (Anagnostou et al., 2020; Cramwinckel et al., 2018; Hansen et al., 2013; Krissansen-Totton & Catling, 2017; Pagani et al., 2010; Rohling et al., 2012; Royer, 2016; Snyder, 2016). In fact, the ESS we estimate for the pre-Quaternary Cenozoic is within the multi-model mean ECS of CMIP6 (3.9°C ± 1.1°C, 68% interval; Zelinka et al., 2020). This indicates that slow feedbacks did not play a significant role in setting the Earth system response to declining external forcing until the middle Pliocene, even after the appearance of the Antarctic ice sheet.

4.5. Exploring State-Dependence of ESS

State-dependence of climate sensitivity to the background climate can arise if climate feedbacks are inconstant in strength under different levels of forcing. For example, water vapor is expected to contribute stronger positive feedbacks to outside radiative perturbation in a warm climate state (Meraner et al., 2013). All else being equal, this would mean that a 1 W/m^2 drop during the early Eocene should induce larger cooling than a 1 W/m^2 drop in the middle Miocene, producing a nonlinear best fit between ΔGST and ΔF. Such a nonlinear state-dependence is often inferred for fast-feedback ECS and is attributed to enhanced feedback contributions from water vapor and cloud microphysics (Anagnostou et al., 2020; Caballero & Huber, 2013; Zhu et al., 2019). On the other hand, ESS is thought to be higher during globally cold intervals because of the amplifying ice-albedo feedback of large ice sheets (Park & Royer, 2011; Stap et al., 2017; Wong et al., 2021).

In addition, more extreme upturns in sensitivity in the form of large-scale climate transitions are also hypothesized to play a role in past climates. Episodes of intense low-latitude glaciation during the Precambrian seem to involve a bifurcation within the ice-albedo feedback that under sufficiently low levels of climate forcing drives a transition into an alternative (globally glaciated) configuration (Hoffman et al., 2017). Sophisticated large-eddy simulations have also identified significant threshold behavior in the atmosphere through increased CO_2 forcing. These thresholds occur through the breakup of subtropical cloud cover and the subsequent loss of surface shading (Schneider et al., 2019), which induce large ΔGST changes (8°C). Schneider et al. (2019) speculated that the termination of a distinct atmospheric state with low cloud cover was responsible for the onset of icehouse conditions at the Eocene–Oligocene boundary.

When examining the preferred parameter case, we do not find clear evidence for either a smooth directional change in ESS under a warmer climate system or an abrupt step-change away from a hothouse. Instead the interval between the early Eocene to middle Pliocene is well described ($r^2 = 0.8$) by a relatively fixed ESS (Figures 6a and 6b).

However, there is a striking offset between the relationship we determined for the pre-Quaternary Cenozoic and the preindustrial. When we extend the linear least squares regression to a forcing of 0 W/m^2, timeslices predict a

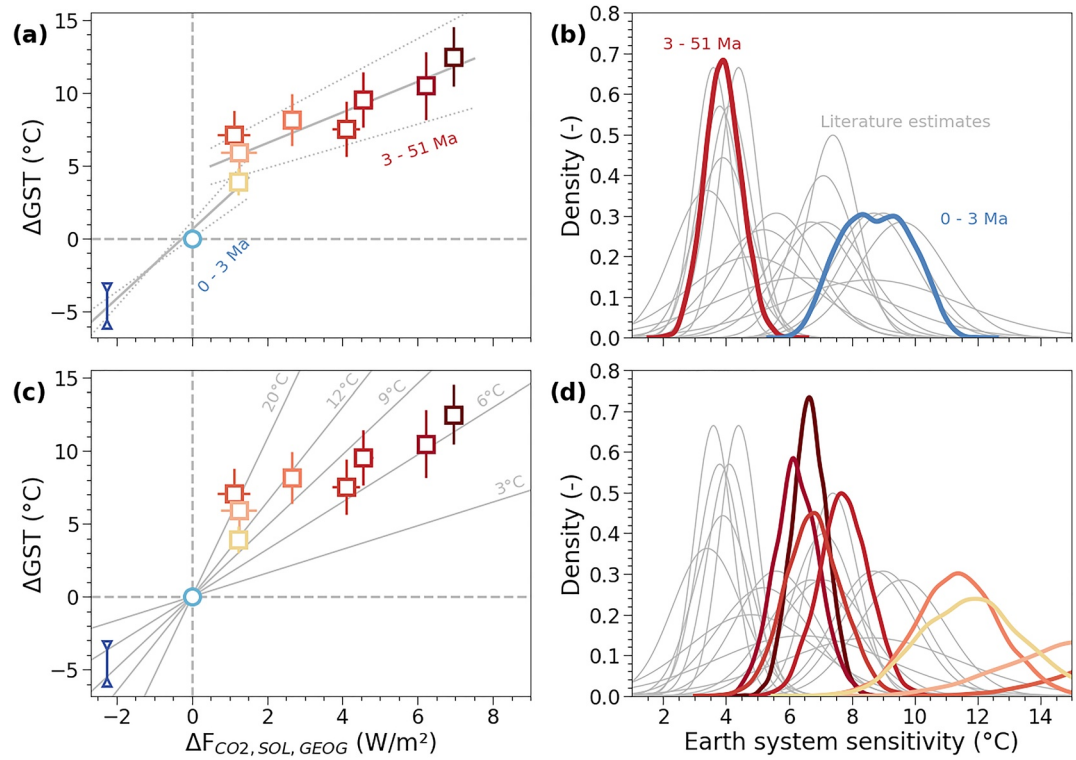

Figure 6. Two alternative ways to interpret past Earth system sensitivity (ESS) from Cenozoic paleoclimate data. (a, c) Identical reconstructed ΔGST and ΔF data using the combination case (Tables 1 and 2), as well as an additional constraint from the Last Glacial Maximum (LGM) without the confounding effect of orbital forcing (dark blue). Uncertainty envelopes (95% confidence interval) of ΔGST and ΔF were propagated from proxy uncertainty using Monte Carlo simulations (n = 5,000). (b, d) The results for an ESS analysis of the same data if ESS is either taken as the relative differences between timeslices or the relative difference between a given timeslice and the preindustrial, respectively.

much warmer climate state (4.5°C ΔGST) than is actually observed (Figure 6a). In other words, cool conditions of the preindustrial are inconsistent with the same ESS that seems to have governed the preceding Cenozoic. This provides a strong case for state-dependence, specifically for a transition toward a regime with an enhanced ESS at some point after the middle Pliocene. Such a transition would also explain the accelerated pace of global cooling we inferred for the Plio-Pleistocene. Average radiative forcing over the last 800 thousand years was just 2 W/m^2 below that of the middle Pliocene (Bereiter et al., 2015) but surface conditions were much colder (Snyder, 2016).

The most salient development of the Plio-Pleistocene is the final culmination of the bipolar icehouse state that Earth occupies today. Stacked benthic oxygen isotope records show a distinct change in trajectory toward enriched values following isotope stage M2 (3.3 million years ago; Westerhold et al., 2020; Figure 5b). A synchronous intensification of glacial indicators from ice-rafted debris to shelf sediment architecture is seen at multiple locations in the North Atlantic and Arctic regions between 2.5 and 2.8 million years ago (De Schepper et al., 2014; Knutz et al., 2019; Rea et al., 2018). These fledgling ice sheets would have provided a strong planetary albedo feedback to declining CO_2 concentrations and thereby could have imparted a high ESS onto the Plio-Pleistocene climate system. Studies that remove the role of ice sheet albedo by including it as an external forcing do not show distinct differences between the early and late Cenozoic (summarized in von der Heydt et al., 2016). Instead, the resulting estimates of paleoclimate sensitivity in these studies ($S_{[CO2,LI]}$) cluster around a common moderate value of 1°C/W/m^2 or 4°C per CO_2 doubling (von der Heydt et al., 2016), similar the ESS value we determine for the pre-Quaternary Cenozoic. This again supports the notion that the implicit inclusion of the ice-albedo feedback is indeed responsible for the Plio-Pleistocene ESS amplification found here.

On shorter timescales, late Pleistocene climate was dominated by large cyclical oscillations in CO_2 concentration, ice sheet size, and ΔGST that were paced by modulations of Earth's orbit. While this is consistent with a more sensitive Earth system, it also poses a problem for quantifying ESS at this time. Orbital variations force the global

climate via their impact on the mass balance of ice sheets. Yet, the sensitivity of ice sheets is nonlinearly related to their volume (Stap et al., 2014) and ice sheets are additionally coupled to variable CO_2 forcing. This means an unknown fraction of glacial-stage ice growth (and thus, ΔGST) is due to orbital forcing that is difficult to disentangle from the ice growth from to lowered CO_2 concentration. Estimating ESS without correcting for the independent role of orbital forcing would bias results toward high values (Schmidt et al., 2017). A conservative estimate of the orbital contribution to ΔGST can be made by considering the better constrained role of ice sheets in general, regardless if their size variations are due to orbital or CO_2 forcing. Recent climate model experiments suggest that the expanded ice sheets of the Last Glacial Maximum (LGM; 18–21 ka) were responsible for half of the global cooling at this time (Erb et al., 2015; Singarayer & Valdes, 2010; Stap et al., 2014). Based on the discussion above and a glacial-stage ΔGST of −6°C (Snyder, 2016; Tierney et al., 2020), it follows that a hypothetical LGM climate which excludes the impact of orbital forcing should have a ΔGST of above −6°C but below −3°C.

In conjunction with the preindustrial and middle Pliocene time periods, these values suggest an ESS of 2.4°C/W/m^2 (±0.6°C/W/m^2, 95% interval) or 8.8°C (±2.2°C/W/m^2, 95% interval) per CO_2 doubling for the last 3 million years (Figures 6a and 6b).

An amplification of ESS in the late Cenozoic has long been suspected (Hansen et al., 2008) but our results are interesting in two respects. First, the glacial amplification factor inferred here (2.2, 1.5–3.4, 95% interval) is on the high end of previous studies which draw on the output of the geological GEOCARB carbon cycle model and favor an amplification factor of about 2 (Park & Royer, 2011; Wong et al., 2021). Second, the transition to higher ESS in GEOCARB is prescribed to occur in the late Eocene (Park & Royer, 2011) due to the rapid emplacement of the Antarctic ice sheet. Our analysis is not able to diagnose an exact breakpoint from low to high ESS (Figure 6) but we can constrain the timing of the onset of higher ESS to no earlier than the Pliocene, some 37 million years later than in GEOCARB.

If ice sheets in the Northern Hemisphere were responsible for a transition in ESS, this begs the question: why did an equivalent regime change not occur following the appearance of ice sheets in the Southern Hemisphere? We speculate that Northern ice sheets had an outsized capacity for positive radiative feedback due to their position at midlatitude. Eurasian ice sheets nucleated at multiple locations in the North Sea down to 52°N and the Laurentide ice sheet reached 39°N as early as 2.4 million years ago (Balco & Rovey, 2010; Batchelor et al., 2019). The majority of Antarctica, by contrast, is contained above 70°S today and has remained in this zone for the entire Cenozoic (Seton et al., 2012). Lower latitudes receive a higher fraction of global insolation, so the expansion or retreat of ice sheets at lower latitudes should have an enhanced impact on the planetary surface albedo and therefore contribute a stronger ice-albedo feedback compared to exclusively polar ice sheets.

4.6. On the Present-Day Vantage Point

The apparent state-change in ESS we infer for the end of the Neogene also carries the potential for significant bias in estimating past ESS if the present-day or preindustrial are imposed as reference values. For example, Steinthorsdottir et al. (2020) recently argued for a high ESS during the middle Miocene based on the coincidence of a warm climate optimum with atmospheric CO_2 concentrations that are only moderately elevated (500 ppm) compared to today. In this case, ESS was defined as the slope between the past climate state and the preindustrial in ΔGST–ΔF space. When we repeat the same point-wise approach with all of our timeslices individually (Figure 6c), we calculate a pronounced increase in ESS of 5°C to >10°C from the Paleogene to the Neogene (Figure 6d). However, this is clearly not an accurate representation of the real evolution of ESS. An increase in ESS between the Paleogene and Neogene would mean that the climate response is more sensitive to the proceeding decline in atmospheric CO_2 and that ΔGST of the Miocene should consequently be well below that of the preceding Oligocene. On the contrary, early Miocene and early Oligocene ΔGST appear to be indistinguishable in our proxy treatment (Figure 5c; Table 1). Since we are able to track the long-term climate development, we find that, using the same parameters as Steinthorsdottir et al. (2020), the middle Miocene is instead more consistent with a moderate to low ESS.

The difference between two given time periods in ΔGST–ΔF space will necessarily be an interpolation of all variations in ESS that may have occurred between these two points. Direct comparison between two given points in time only approximates the true behavior of the Earth system if ESS has remained constant during the elapsed

time interval. Our results however show that most of the Cenozoic appears to have operated in a ESS regime different from that of the Quaternary (Figures 6a and 6b). Anchoring one pre-Quaternary time period against the preindustrial therefore runs the risk of significant bias in estimating ESS since both time periods only came about through a transition from one ESS regime to another. Put another way, the coexistence of elevated ΔGST and near-modern ΔF in the past does not imply high ESS on its own because these conditions can also arise from a warm preexisting climate system that responded with low ESS to a reduction of ΔF.

4.7. Limitations and Caveats

Both ΔGST and ΔF were estimated through a multiproxy approach based on the idea that a balance of methods should provide the least biased representation of the past. For example, we noted a pervasive discrepancy between geochemical marine and paleobotanical continental proxies (Figure 3) but included both in our ΔGST calculation (at least outside tropical paleolatitudes) as there is no consensus yet on the origin of this pattern. However, we note that there are several possible biases which are not explicitly taken into account here.

ΔGST estimates correct for ΔT from major collisional belts but a topographic control may have also controlled ice sheet extent (Paxman et al., 2020) and therefore the strength of the slow ice-albedo feedback in the past. Since this effect is quasi-independent of the climate state, the topographic evolution of subglacial bedrock is a forcing factor external to the climate system, similar to, for example, solar brightening. We do not apply a correction for this effect.

Averaging of geologic proxies within a discrete number of intervals, as we do here, further assumes that the paleoclimate state was constant within each timeslice. This is unlikely to hold true for timeslices with long duration like the early Eocene (7 million years) or the early Oligocene (6.1 million years). Median estimates reported here could be biased if proxies are not homogeneously distributed within each timeslice. Whether this is the case or not is difficult to resolve for ΔT data owing to the poor constraints on the age of most terrestrial sites. Atmospheric CO_2 data from phytoplankton $\delta^{13}C$ and calcite $\delta^{11}B$ data tend to have more refined age modeling and cover most timeslices at a density of >7 samples per million years. One notable exception is the early Oligocene where the proxy density is low (5 samples per million years) and a gap in boron isotopic data from 33 to 24 million years (Greenop et al., 2019) means that $\delta^{11}B$-based CO_2 is concentrated at the beginning of the timeslice, when CO_2 was still high. As a consequence, the true median atmospheric CO_2 (and thus ΔF_{CO2}) of the early Oligocene may be overestimated here.

Due to the wide range and number of climate states included in our analysis, ESS results for the Paleogene and Neogene are not strongly dependent on the position of a given data point. In contrast, Plio-Pleistocene ESS is constrained by us through only three different time periods, namely the middle Pliocene, the preindustrial, and the LGM. These only cover a smaller ΔF range of 3 W/m^2 (compared to 6 W/m^2 for the remaining Cenozoic) and so provide less leverage to estimate ESS. In addition, the logarithmic relationship between CO_2 and ΔF implies that small deviations at low CO_2 concentrations will yield substantial differences in ΔF. For example, the multiproxy CO_2 estimate we rely on for the middle Pliocene only differs from the average $\delta^{11}B$-based CO_2 by 40 ppm, yet this is equivalent to a difference in ΔF of 0.7 W/m^2 (Table 2)—a complication that is not equally true for the LGM and preindustrial as CO_2 concentrations of these periods are known from the ice core record. While amplification of ESS is required by the anomalously cold preindustrial conditions compared to the pre-Quaternary, these caveats limit the precision at which we can place quantitative bounds on ESS of the Plio-Pleistocene.

4.8. Implications for Future Warming

The magnitude and behavior of ESS we reconstruct for the Cenozoic has implications for the long-term response of the Earth system to carbon release occurring today. Following our interpretation above, we suggest that Earth is still within a high-ESS regime and that the future decay of ice masses in the Northern Hemisphere should propel the Arctic into a warmer state. Timeslices suggest that stabilization at a present-day net anthropogenic forcing (2 W/m^2; von Schuckmann et al., 2016) would result in an asymptotic relaxation of the climate system toward a ΔGST of >3°C over the next millennia (Figure 6). This implies that instrumentally observed warming (1°C) represents only a fraction of the final equilibrium temperature response expected for Earth. The present-day atmospheric composition may thus be consistent with the ΔGST limit of 2°C set by the Paris climate accords (Schellnhuber et al., 2016) on a centennial timescale but severely exceed it on a longer-term basis. In fact, in

order to keep within the 2°C ΔGST limit on a long-term, atmospheric concentrations would need to stay below 350 ppm in CO_2-equivalent, providing matching deep-time evidence in favor of existing proposals to limit CO_2 concentrations to the same value (https://350.org/).

Lastly, human interference with the Earth system is occurring at an unusually fast pace (Zeebe et al., 2016) and has already subjected much of Earth's surface to extensive ecosystem degradation over the last centuries (Barnosky et al., 2012), signaling the potential onset of the sixth mass extinction event in Earth history (Ceballos et al., 2017). Some environmental mechanisms which in the geologic past have buffered against abrupt environmental changes may not be fully functional today due to anthropogenic interference. On the other hand, recovery of the Earth system from abrupt carbon release may be more efficient today than it was in the distant past (Rugenstein et al., 2019). Given the unique circumstances of the Anthropocene, the question as to whether the Earth system response could diverge from its behavior during equilibrium states in the Cenozoic may be, to a large degree, intractable.

5. Conclusions

We assimilated long-term Cenozoic changes in surface temperature in combination with coeval atmospheric CO_2 concentration to produce a parsimonious constraint on ESS to forcing by greenhouse gases, solar brightness, and continental drift. On average, past temperature changes are strongly concentrated at high latitude, which were ≥20°C warmer than today for much of the Cenozoic, while changes in the tropics are comparatively subdued. ESS appears to have been nearly constant at a low value from the early Eocene to middle Pliocene but we find that the same ESS is inconsistent with cool conditions of the preindustrial. We interpret this as a sign that the climate system transitioned into a regime with high ESS at some point within the last 3 million years, possibly due to the appearance of ice sheets in the Northern Hemisphere. Finally, in the context of future, anthropogenically forced climate change, our results stress the importance of mitigation approaches because a sensitive Earth system would yield long-term levels of global warmth that are well outside the bounds of recent human history and may exceed adaptive capabilities for much of the global population (Mora et al., 2017).

Conflict of Interest

The authors declare no conflicts of interest relevant to this study.

Data Availability Statement

The proxy data compilation on which this paper is based is publicly available at GFZ Data Services (Ring et al., 2022).

Acknowledgments
Michael J. Henehan and Zhengfei Guo are thanked for useful discussion on the manuscript. We also thank the four anonymous reviewers and Matthew Huber for constructive comments. This study was partially supported by the German Science Foundation priority program EarthShape: Earth Surface Shaping by Biota (SPP, 1801) Grants EH329/14-2 and EH329/23-1 to T.A.E and MU4188/3-1 and MU4188/1-1 to S.G.M. We also acknowledge support from the Open Access Publishing Fund of the University of Tübingen. Open Access funding enabled and organized by Projekt DEAL.

References

Anagnostou, E., John, E. H., Babila, T. L., Sexton, P. F., Ridgwell, A., Lunt, D. J., et al. (2020). Proxy evidence for state-dependence of climate sensitivity in the Eocene greenhouse. *Nature Communications*, *11*(1), 4436. https://doi.org/10.1038/s41467-020-17887-x

Anagnostou, E., John, E. H., Edgar, K. M., Foster, G. L., Ridgwell, A., Inglis, G. N., et al. (2016). Changing atmospheric CO_2 concentration was the primary driver of early Cenozoic climate. *Nature*, *533*(7603), 380–384. https://doi.org/10.1038/nature17423

Anderson, J. B., Warny, S., Askin, R. A., Wellner, J. S., Bohaty, S. M., Kirshner, A. E., et al. (2011). Progressive Cenozoic cooling and the demise of Antarctica's last refugium. *Proceedings of the National Academy of Sciences of the United States of America*, *108*(28), 11356–11360. https://doi.org/10.1073/pnas.1014885108

Baatsen, M., von der Heydt, A. S., Huber, M., Kliphuis, M. A., Bijl, P. K., Sluijs, A., & Dijkstra, H. A. (2020). The middle to late Eocene greenhouse climate modelled using the CESM 1.0.5. *Climate of the Past*, *16*(6), 2573–2597. https://doi.org/10.5194/cp-16-2573-2020

Balco, G., & Rovey, C. W. (2010). Absolute chronology for major Pleistocene advances of the Laurentide ice sheet. *Geology*, *38*(9), 795–798. https://doi.org/10.1130/g30946.1

Ballantyne, A. P., Greenwood, D. R., Damsté, J. S. S., Csank, A. Z., Eberle, J. J., & Rybczynski, N. (2010). Significantly warmer Arctic surface temperatures during the Pliocene indicated by multiple independent proxies. *Geology*, *38*(7), 603–606. https://doi.org/10.1130/g30815.1

Barnes, J. B., & Ehlers, T. A. (2009). End member models for Andean plateau uplift. *Earth-Science Reviews*, *97*(1–4), 105–132. https://doi.org/10.1016/j.earscirev.2009.08.003

Barnosky, A. D., Hadly, E. A., Bascompte, J., Berlow, E. L., Brown, J. H., Fortelius, M., et al. (2012). Approaching a state shift in Earth's biosphere. *Nature*, *486*(7401), 52–58. https://doi.org/10.1038/nature11018

Barrett, P. J. (2013). Resolving views on Antarctic glacial history—The Sirius debate. *Earth and Environmental Science Transactions of the Royal Society of Edinburgh*, *104*(1), 31–53. https://doi.org/10.1017/s175569101300008x

Batchelor, C. L., Margold, M., Krapp, M., Murton, D. K., Dalton, A. S., Gibbard, P. L., et al. (2019). The configuration of Northern Hemisphere ice sheets through the Quaternary. *Nature Communications*, *10*(1), 3713. https://doi.org/10.1038/s41467-019-11601-2

Batenburg, S. J., Voigt, S., Friedrich, O., Osborne, A. H., Bornemann, A., Klein, T., et al. (2018). Major intensification of Atlantic overturning circulation at the onset of Paleogene greenhouse warmth. *Nature Communications*, *9*(1), 4954. https://doi.org/10.1038/s41467-018-07457-7

Bereiter, B., Eggleston, S., Schmitt, J., Nehrbass-Ahles, C., Stocker, T. F., Fischer, H., et al. (2015). Revision of the EPICA Dome C CO_2 record from 800 to 600 kyr before present. *Geophysical Research Letters*, *42*, 542–549. https://doi.org/10.1002/2014GL061957

Bijl, P. K., Bendle, J. A. P., Bohaty, S. M., Pross, J., Schouten, S., Tauxa, L., et al., 318 Scientists. (2013). Eocene cooling linked to early flow across the Tasmanian Gateway. *Proceedings of the National Academy of Sciences of the United States of America*, *110*(24), 9645–9650. https://doi.org/10.1073/pnas.1220872110

Bjorkman, A. D., Myers-Smith, I.-H., Elmendorf, S. C., Normand, S., Rüger, N., Beck, P. S. A., et al. (2018). Plant functional trait change across a warming tundra biome. *Nature*, *562*, 57–62. https://doi.org/10.1038/s41586-018-0563-7

Botsyun, S., Sepulchre, P., Donnadieu, Y., Risi, C., Licht, A., & Rugenstein, J. K. C. (2019). Revised paleoaltimetry data show low Tibetan plateau elevation during the Eocene. *Science*, *363*(6430), aaq1436. https://doi.org/10.1126/science.aaq1436

Burls, N. J., Bradshaw, C. D., De Boer, A. M., Herold, N., Huber, M., Pound, M., et al. (2021). Simulating Miocene warmth: Insights from an opportunistic multi-model ensemble (MioMIP1). *Paleoceanography and Paleoclimatology*, *36*, e2020PA004054. https://doi.org/10.1029/2020PA004054

Byrne, M. P., & O'Gorman, P. A. (2018). Trends in continental temperature and humidity directly linked to ocean warming. *Proceedings of the National Academy of Sciences of the United States of America*, *115*(19), 4863–4868. https://doi.org/10.1073/pnas.1722312115

Caballero, R., & Huber, M. (2013). State-dependent climate sensitivity in past warm climates and its implications for future climate projections. *Proceedings of the National Academy of Sciences of the United States of America*, *110*(35), 14162–14167. https://doi.org/10.1073/pnas.1303365110

Carter, A., Riley, T. R., Hillenbrand, C.-D., & Rittner, M. (2017). Widespread Antarctic glaciation during the late Eocene. *Earth and Planetary Science Letters*, *458*, 49–57. https://doi.org/10.1016/j.epsl.2016.10.045

Ceballos, G., Ehrlich, P. R., & Dirzo, R. (2017). Biological annihilation via the ongoing sixth mass extinction signaled by vertebrate population losses and declines. *Proceedings of the National Academy of Sciences of the United States of America*, *114*(30), E6089–E6096. https://doi.org/10.1073/pnas.1704949114

Contreras, L., Pross, J., Bijl, P. K., O'Hara, R. B., Raine, J. I., Sluijs, A., & Brinkhuis, H. (2014). Southern high-latitude terrestrial climate change during the Palaeocene–Eocene derived from a marine pollen record (ODP Site 1172, East Tasman Plateau). *Climate of the Past*, *10*(4), 1401–1420. https://doi.org/10.5194/cp-10-1401-2014

Cramer, B. S., Miller, K. G., Barrett, P. J., & Wright, J. D. (2011). Late Cretaceous–Neogene trends in deep ocean temperature and continental ice volume: Reconciling records of benthic foraminiferal geochemistry ($\delta^{18}O$ and Mg/Ca) with sea level history. *Journal of Geophysical Research*, *116*, C12023. https://doi.org/10.1029/2011JC007255

Crampton-Flood, E. D., Tierney, J. E., Peterse, F., Kirkels, F. M. S. A., & Damsté, J. S. S. (2020). BayMBT: A Bayesian calibration model for branched glycerol dialkyl glycerol tetraethers in soils and peats. *Geochimica et Cosmochimica Acta*, *268*, 142–159. https://doi.org/10.1016/j.gca.2019.09.043

Cramwinckel, M. J., Huber, M., Kocken, I. J., Agnini, C., Bijl, P. K., Bohaty, S. M., et al. (2018). Synchronous tropical and polar temperature evolution in the Eocene. *Nature*, *559*(7714), 382–386. https://doi.org/10.1038/s41586-018-0272-2

Davies, A., Hunter, S. J., Gréselle, B., Haywood, A. M., & Robson, C. (2019). Evidence for seasonality in early Eocene high latitude sea-surface temperatures. *Earth and Planetary Science Letters*, *519*, 274–283. https://doi.org/10.1016/j.epsl.2019.05.025

De Nooijer, L. J., van Dijk, I., Toyofuku, T., & Reichart, G. J. (2017). The impacts of seawater Mg/Ca and temperature on element incorporation in benthic foraminiferal calcite. *Geochemistry, Geophysics, Geosystems*, *18*, 3617–3630. https://doi.org/10.1002/2017GC007183

De Schepper, S., Gibbard, P. L., Salzmann, U., & Ehler, J. (2014). A global synthesis of the marine and terrestrial evidence for glaciation during the Pliocene epoch. *Earth-Science Reviews*, *135*, 83–102. https://doi.org/10.1016/j.earscirev.2014.04.003

Erb, M. P., Jackson, C. S., & Broccoli, A. J. (2015). Using single-forcing GCM simulations to reconstruct and interpret Quaternary climate change. *Journal of Climate*, *28*(24), 9746–9767. https://doi.org/10.1175/JCLI-D-15-0329.1

Evans, D., Erez, J., Oron, S., & Müller, W. (2015). Mg/Ca-temperature and seawater-test chemistry relationships in the shallow-dwelling large benthic foraminifera *Operculina ammonoides*. *Geochimica et Cosmochimica Acta*, *148*, 325–342. https://doi.org/10.1016/j.gca.2014.09.039

Fan, M., Hough, B. G., & Passey, B. H. (2014). Middle to late Cenozoic cooling and high topography in the central Rocky Mountains: Constraints from clumped isotope geochemistry. *Earth and Planetary Science Letters*, *408*, 35–47. https://doi.org/10.1016/j.epsl.2014.09.050

Farnsworth, A., Lunt, D. J., O'Brien, C. L., Foster, G. L., Inglis, G. N., Markwick, P., et al. (2019). Climate sensitivity on geological timescales controlled by nonlinear feedbacks and ocean circulation. *Geophysical Research Letters*, *46*, 9880–9889. https://doi.org/10.1029/2019GL083574

Fielding, C. R. (2018). Stratigraphic architecture of the Cenozoic succession in the McMurdo Sound region, Antarctica: An archive of polar palaeoenvironmental change in a failed rift setting. *Sedimentology*, *65*, 1–61. https://doi.org/10.1111/sed.12413

Foster, G. L., & Rae, J. W. B. (2016). Reconstructing ocean pH with boron isotopes in foraminifera. *Annual Review of Earth and Planetary Sciences*, *44*(1), 207–237. https://doi.org/10.1146/annurev-earth-060115-012226

Francis, J. E., & Hill, R. S. (1996). Fossil plants from the Pliocene Sirius Group, Transantarctic Mountains: Evidence for climate from growth rings and fossil leaves. *PALAIOS*, *11*(4), 389–396. https://doi.org/10.2307/3515248

Garbe, J., Albrecht, T., Levermann, A., Donges, J. F., & Winkelmann, R. (2020). The hysteresis of the Antarctic ice sheet. *Nature*, *585*(7826), 538–544. https://doi.org/10.1038/s41586-020-2727-5

Goldner, A., Huber, M., & Caballero, R. (2013). Does Antarctic glaciation cool the world? *Climate of the Past*, *9*(1), 173–189. https://doi.org/10.5194/cp-9-173-2013

Gough, D. O. (1981). Solar interior structure and luminosity variations. *Solar Physics*, *74*(1), 21–34. https://doi.org/10.1007/bf00151270

Greenop, R., Sosdian, S. M., Henehan, M. J., Wilson, P. A., Lear, C. H., & Foster, G. L. (2019). Orbital forcing, ice volume, and CO_2 across the Oligocene–Miocene transition. *Paleoceanography and Paleoclimatology*, *34*, 316–328. https://doi.org/10.1029/2018PA003420

Grimm, G. W., Bouchal, J. M., Denk, T., & Potts, A. (2016). Fables and foibles: A critical analysis of the Palaeoflora database and the coexistence approach for palaeoclimate reconstruction. *Review of Paleobotany and Palynology*, *233*, 216–235. https://doi.org/10.1016/j.revpalbo.2016.07.001

Grimm, G. W., & Potts, A. J. (2016). Fallacies and fantasies: The theoretical underpinnings of the coexistence approach for palaeoclimate reconstruction. *Climate of the Past*, *12*(3), 611–622. https://doi.org/10.5194/cp-12-611-2016

Gulick, S. P. S., Shevenell, A. E., Montelli, A., Fernandez, R., Smith, C., Warny, S., et al. (2017). Initiation and long-term instability of the East Antarctic ice sheet. *Nature*, *552*(7684), 225–229. https://doi.org/10.1038/nature25026

Hansen, J., Sato, M., Kharecha, P., Beerling, D., Berner, R., Masson-Delmotte, V., et al. (2008). Target atmospheric CO_2: Where should humanity aim? *The Open Atmospheric Science Journal*, *2*(1), 217–231. https://doi.org/10.2174/1874282300802010217

Hansen, J., Sato, M., Russell, G., & Kharecha, P. (2013). Climate sensitivity, sea level and atmospheric carbon dioxide. *Philosophical Transactions of the Royal Society A*, *371*(2001), 20120294. https://doi.org/10.1098/rsta.2012.0294

Haywood, A. M., Tindall, J. C., Dowsett, H. J., Dolan, A. M., Foley, K. M., Hunter, S. J., et al. (2020). The Pliocene Model Intercomparison Project Phase 2: Large-scale climate features and climate sensitivity. *Climate of the Past*, *16*(6), 2095–2123. https://doi.org/10.5194/cp-16-2095-2020

Hoffman, P. F., Abbot, D. S., Ashkenazy, Y., Benn, D. I., Brocks, J. J., Cohen, P. A., et al. (2017). Snowball Earth climate dynamics and Cryogenian geology–geobiology. *Science Advances*, *3*(11), e1600983. https://doi.org/10.1126/sciadv.1600983

Hollis, C. J., Taylor, K. W. R., Handley, L., Pancost, R. D., Huber, M., Creech, J. B., et al. (2012). Early Paleogene temperature history of the southwest Pacific Ocean: Reconciling proxies and models. *Earth and Planetary Science Letters*, *350*, 53–66. https://doi.org/10.1016/j.epsl.2012.06.024

Huang, J., Yu, H., Guan, X., Wang, G., & Guo, R. (2015). Accelerated dryland expansion under climate change. *Nature Climate Change*, *6*(2), 166–171. https://doi.org/10.1038/nclimate2837

Huck, C. E., van de Flierdt, T., Bohaty, S. M., & Hammond, S. J. (2017). Antarctic climate, Southern Ocean circulation patterns and deep water formation during the Eocene. *Paleoceanography and Paleoclimatology*, *32*, 674–691. https://doi.org/10.1002/2017PA003135

Inglis, G. N., Bragg, F., Burls, N. J., Cramwinckel, M. J., Evans, D., Foster, G. L., et al. (2020). Global mean surface temperature and climate sensitivity of the early Eocene climatic optimum (EECO), Paleocene–Eocene thermal maximum (PETM), and latest Paleocene. *Climate of the Past*, *16*(5), 1953–1968. https://doi.org/10.5194/cp-16-1953-2020

Kennedy, K. T., Farnsworth, A., Lunt, D. J., Lear, C. H., & Markwick, P. J. (2015). Atmospheric and oceanic impacts of Antarctic glaciation across the Eocene–Oligocene transition. *Philosophical Transactions of the Royal Society A*, *373*(2054), 20140419. https://doi.org/10.1098/rsta.2014.0419

Knobbe, T. K., & Schaller, M. F. (2018). A tight coupling between atmospheric pCO_2 and sea-surface temperature in the Late Triassic. *Geology*, *46*(1), 43–46. https://doi.org/10.1130/g39405.1

Knutti, R., Rugenstein, M. A. A., & Hegerl, G. C. (2017). Beyond equilibrium climate sensitivity. *Nature Geoscience*, *10*, 727–736. https://doi.org/10.1038/ngeo3017

Knutz, P. C., Newton, A. M. W., Hopper, J. R., Huuse, M., Gregersen, U., Sheldon, E., & Dybjær, K. (2019). Eleven phases of Greenland ice sheet shelf-edge advance over the past 2.7 million years. *Nature Geoscience*, *12*(5), 361–368. https://doi.org/10.1038/s41561-019-0340-8

Konrad, W., Royer, D. L., Franks, P. J., & Roth-Nebelsick, A. (2020). Quantitative critique of leaf-based paleo-CO_2 proxies: Consequence for their reliability and applicability. *Geologic Journal*, *56*(2), 886–902. https://doi.org/10.1002/gj.3807

Krissansen-Totton, J., & Catling, D. C. (2017). Constraining climate sensitivity and continental versus seafloor weathering using an inverse geologic carbon cycle model. *Nature Communications*, *8*(1), 15423. https://doi.org/10.1038/ncomms15423

Kump, L. R., & Pollard, D. (2008). Amplification of Cretaceous warmth by biological cloud feedbacks. *Science*, *320*(5873), 195. https://doi.org/10.1126/science.1153883

Lacis, A. A., Schmidt, G. A., Rind, D., & Ruedy, R. A. (2010). Atmospheric CO_2: Principal control knob governing Earth's temperature. *Science*, *330*(6002), 356–359. https://doi.org/10.1126/science.1190653

Lear, C. H., Coxall, H. K., Foster, G. L., Lunt, D. J., Mawbey, E. M., Rosenthal, Y., et al. (2015). Neogene ice volume and ocean temperatures: Insights from infaunal foraminiferal Mg/Ca paleothermometry. *Paleoceanography and Paleoclimatology*, *30*, 1437–1454. https://doi.org/10.1002/2015PA002833

Levy, R., Harwood, D., Florindo, F., Sangiorgi, F., Tripati, R., von Eynatten, H., et al. (2016). Antarctic ice sheet sensitivity to atmospheric CO_2 variations in the early to mid-Miocene. *Proceedings of the National Academy of the United States of America*, *113*(13), 3453–3458. https://doi.org/10.1073/pnas.1516030113

Lewis, A. R., Marchant, D. R., Ashworth, A. C., Hedenäs, L., Hemming, S. R., Johnson, J. V., et al. (2008). Mid-Miocene cooling and the extinction of tundra in continental Antarctica. *Proceedings of the National Academy of Sciences of the United States of America*, *105*(31), 10676–10680. https://doi.org/10.1073/pnas.0802501105

Liebrand, D., de Bakker, A. T. M., Beddow, H. M., Wilson, P. A., Bohaty, S. M., Ruessink, G., et al. (2017). Evolution of the early Antarctic ice ages. *Proceedings of the National Academy of Sciences of the United States of America*, *114*(15), 3867–3872. https://doi.org/10.1073/pnas.1615440114

Lunt, D. J., Haywood, A. M., Schmidt, G. A., Salzmann, U., Valdes, P. J., & Dowsett, H. J. (2010). Earth system sensitivity inferred from Pliocene modelling and data. *Nature Geoscience*, *3*(1), 60–64. https://doi.org/10.1038/ngeo706

Macdonald, F. A., Swanson-Hysell, N. L., Park, Y., Lisiecki, L., & Jagoutz, O. (2019). Arc-continent collisions in the tropics set Earth's climate state. *Science*, *364*(6436), 181–184. https://doi.org/10.1126/science.aav5300

Malevich, S. B., Vetter, L., & Tierney, J. E. (2019). Global core top calibration of $\delta^{18}O$ in planktic foraminifera to sea surface temperature. *Paleoceanography and Paleoclimatology*, *34*, 1292–1315. https://doi.org/10.1029/2019PA003576

Marschalek, J. W., Zurli, L., Talarico, F., van der Flierdt, T., Vermeesch, P., Carter, A., et al. (2021). A large West Antarctic ice sheet explains early Neogene sea-level amplitude. *Nature*, *600*(7889), 450–455. https://doi.org/10.1038/s41586-021-04148-0

Martínez-Botí, M. A., Foster, G. L., Chalk, T. B., Rohling, E. J., Sexton, P. F., Lunt, D. J., et al. (2015). Plio-Pleistocene climate sensitivity evaluated using high-resolution CO_2 records. *Nature*, *518*(7537), 49–54. https://doi.org/10.1038/nature14145

McKay, R., Naish, T., Carter, L., Riesselman, C., Dunbar, R., Sjunneskog, C., et al. (2012). Antarctic and Southern Ocean influences on late Pliocene global cooling. *Proceedings of the National Academy of Sciences of the United States of America*, *109*(17), 6423–6428. https://doi.org/10.1073/pnas.1112248109

Meckler, A. N., Sexton, P. F., Piasecki, A. M., Leutert, T. J., Marquardt, J., Ziegler, M., et al. (2022). Cenozoic evolution of deep ocean temperature from clumped isotope thermometry. *Science*, *377*, 86–90. https://doi.org/10.1126/science.abk0604

Meraner, K., Mauritsen, T., & Voigt, A. (2013). Robust increase in equilibrium climate sensitivity under global warming. *Geophysical Research Letters*, *40*, 5944–5948. https://doi.org/10.1002/2013GL058118

Modestou, S. E., Leutert, T. J., Fernandez, A., Lear, C. H., & Meckler, A. N. (2021). Warm middle Miocene Indian Ocean Bottom Water temperatures: Comparison of clumped isotope and Mg/Ca-based estimates. *Paleoceanography and Paleoclimatology*, *35*, e2020PA003927. https://doi.org/10.1029/2020PA003927

Mora, C., Dousset, B., Caldwell, I. R., Powell, F. E., Geronimo, R. C., Bielecki, C. R., et al. (2017). Global risk of deadly heat. *Nature Climate Change*, *7*, 501–506. https://doi.org/10.1038/nclimate3322

Myhre, G., Highwood, E. J., Shine, K. P., & Stordal, F. (1998). New estimates of radiative forcing due to well mixed greenhouse gases. *Geophysical Research Letters*, *25*(14), 2715–2718. https://doi.org/10.1029/98GL01908

O'Brien, C. L., Huber, M., Thomas, E., Pagani, M., Super, J. R., Elder, L. E., & Hull, P. M. (2020). The enigma of Oligocene climate and global surface temperature evolution. *Proceedings of the National Academy of Sciences of the United States of America*, *117*(41), 25302–25309. https://doi.org/10.1073/pnas.2003914117

O'Brien, C. L., Robinson, S. A., Pancost, R. D., Damsté, J. S. S., Schouten, S., Lunt, D. J., et al. (2017). Cretaceous sea-surface temperature evolution constraints from TEX_{86} and planktonic foraminiferal oxygen isotopes. *Earth-Science Reviews*, *172*, 224–247. https://doi.org/10.1016/j.earscirev.2017.07.012

Pagani, M., Liu, Z., LaRiviere, J., & Ravelo, A. C. (2010). High Earth-system climate sensitivity determined from Pliocene carbon dioxide concentrations. *Nature Geoscience*, *3*(1), 27–30. https://doi.org/10.1038/ngeo724

Page, M., Licht, A., Dupont-Nivet, G., Meijer, N., Barbolini, N., Hoorn, C., et al. (2019). Synchronous cooling and decline in monsoonal rainfall in northeastern Tibet during the fall into the Oligocene icehouse. *Geology*, *47*(3), 203–206. https://doi.org/10.1130/g45480.1

Park, J., & Royer, D. L. (2011). Geologic constraints on the glacial amplification of Phanerozoic climate sensitivity. *American Journal of Science*, *311*, 1–26. https://doi.org/10.2475/01.2011.01

Paxman, G. J. G., Gasson, E. G. W., Jamieson, S. S. R., Bentley, M. J., & Ferraccioli, F. (2020). Long-term increase in Antarctic ice sheet vulnerability driven by bed topography evolution. *Geophysical Research Letters*, *47*, e2020GL090003. https://doi.org/10.1029/2020GL090003

Pross, J., Contreras, L., Bijl, P. K., Greenwood, D. R., Bohaty, S. M., Schouten, S., et al., Integrated Ocean Drilling Program Expedition 318 Scientists. (2012). Persistent near-tropical warmth on the Antarctic continent during the early Eocene epoch. *Nature*, *488*(7409), 73–77. https://doi.org/10.1038/nature11300

Rae, J. W. B., Zhang, Y. G., Liu, X., Foster, G. L., Stoll, H. M., & Whiteford, R. D. M. (2021). Atmospheric CO_2, over the past 66 million years from marine archives. *Annual Review of Earth and Planetary Sciences*, *49*(1), 609–641. https://doi.org/10.1146/annurev-earth-082420-063026

Rea, B. R., Newton, A. M. W., Lamb, R. M., Harding, R., Bigg, G. R., Rose, P., et al. (2018). Extensive marine-terminating ice sheets in Europe from 2.5 million years ago. *Science Advances*, *4*(6), eaar8327. https://doi.org/10.1126/sciadv.aar8327

Ring, S. J., Mutz, S. G., & Ehlers, T. A. (2022). Compilation of Cenozoic temperature proxies for terrestrial and marine surface environments [Dataset]. GFZ Data Services. https://doi.org/10.5880/GFZ.3.3.2022.005

Rohling, E. J., Sluijs, A., Dijkstra, H. A., Köhler, P., van de Wal, R. S. W., von der Heydt, A. S., et al. (2012). Making sense of palaeoclimate sensitivity. *Nature*, *491*(7426), 683–691. https://doi.org/10.1038/nature11574

Royer, D. L. (2016). Climate sensitivity in the geologic past. *Annual Review of Earth and Planetary Science*, *44*(1), 277–293. https://doi.org/10.1146/annurev-earth-100815-024150

Rugenstein, J. K. C., Ibarra, D. E., & von Blanckenburg, F. (2019). Neogene cooling driven by land surface reactivity rather than increased weathering fluxes. *Nature*, *571*(7763), 99–102. https://doi.org/10.1038/s41586-019-1332-y

Schellnhuber, H. J., Rahmstorf, S., & Winkelmann, R. (2016). Why the right climate target was agreed in Paris. *Nature Climate Change*, *6*(7), 649–653. https://doi.org/10.1038/nclimate3013

Schmidt, G. A., Severinghaus, J., Abe-Ouchi, A., Alley, R. B., Broecker, W., Brook, E., et al. (2017). Overestimate of committed warming. *Nature*, *547*(7662), E16–E17. https://doi.org/10.1038/nature22803

Schneider, T., Kaul, C. M., & Pressel, K. G. (2019). Possible climate transitions from breakup of stratocumulus decks under greenhouse warming. *Nature Geoscience*, *12*(3), 163–167. https://doi.org/10.1038/s41561-019-0310-1

Seidel, S. D., & Yang, D. (2020). The lightness of water vapor helps to stabilize tropical climate. *Science Advances*, *6*(19), eaba1951. https://doi.org/10.1126/sciadv.aba1951

Seton, M., Müller, R. D., Zahirovic, S., Gaina, C., Torsvik, T., Shephard, G., et al. (2012). Global continental and ocean basin reconstructions since 200 Ma. *Earth-Science Reviews*, *113*(3–4), 212–270. https://doi.org/10.1016/j.earscirev.2012.03.002

Sherwood, S. C., Webb, M. J., Annan, J. D., Armour, K. C., Forster, P. M., Hargreaves, J. C., et al. (2020). An assessment of Earth's climate sensitivity using multiple lines of evidence. *Reviews of Geophysics*, *58*, e2019RG000678. https://doi.org/10.1029/2019RG000678

Singarayer, J. S., & Valdes, P. J. (2010). High-latitude climate sensitivity to ice-sheet forcing over the last 120 kyr. *Quaternary Science Reviews*, *29*(1–2), 43–55. https://doi.org/10.1016/j.quascirev.2009.10.011

Snyder, C. W. (2016). Evolution of global temperature over the past two million years. *Nature*, *538*(7624), 226–228. https://doi.org/10.1038/nature19798

Sosdian, S. M., Greenop, R., Hain, H. P., Foster, G. L., Pearson, P. N., & Lear, C. H. (2018). Constraining the evolution of Neogene ocean carbonate chemistry using the boron isotope pH proxy. *Earth and Planetary Science Letters*, *498*, 362–376. https://doi.org/10.1016/j.epsl.2018.06.017

Stap, L. B., van de Wal, R. S. W., de Boer, B., Bintanja, R., & Lourens, L. J. (2014). Interaction of ice sheets and climate during the past 800 000 years. *Climate of the Past*, *10*(6), 2135–2152. https://doi.org/10.5194/cp-10-2135-2014

Stap, L. B., van de Wal, R. S. W., de Boer, B., Bintanja, R., & Lourens, L. J. (2017). The influence of ice sheets on temperature during the past 38 million years inferred from a one-dimensional ice sheet-climate model. *Climate of the Past*, *13*(9), 1243–1257. https://doi.org/10.5194/cp-13-1243-2017

Steinthorsdottir, M., Jardine, P. E., & Rember, W. C. (2020). Near-future pCO_2 during the hot Miocene climatic optimum. *Paleoceanography and Paleoclimatology*, *36*, e2020PA003900. https://doi.org/10.1029/2020PA003900

Suan, G., Popescu, S.-M., Suc, J.-P., Schnyder, J., Fauquette, S., Baudin, F., et al. (2017). Subtropical climate conditions and mangrove growth in Arctic Siberia during the early Eocene. *Geology*, *45*(6), 539–542. https://doi.org/10.1130/g38547.1

Sutton, R. T., Dong, B., & Gregory, J. M. (2007). Land/sea warming ratio in response to climate change: IPCC AR4 model results and comparison with observations. *Geophysical Research Letters*, *34*, L02701. https://doi.org/10.1029/2006GL028164

Tierney, J. E., Malevich, S. B., Gray, W., Vetter, L., & Thirumalai, K. (2019). Bayesian calibration of the Mg/Ca paleothermometer in planktic foraminifera. *Paleoceanography and Paleoclimatology*, *34*, 2005–2030. https://doi.org/10.1029/2019PA003744

Tierney, J. E., & Tingley, M. P. (2014). A Bayesian, spatially-varying calibration model for the TEX_{86} proxy. *Geochimica et Cosmochimica Acta*, *127*, 83–106. https://doi.org/10.1016/j.gca.2013.11.026

Tierney, J. E., & Tingley, M. P. (2018). BAYSPLINE: A new calibration for the alkenone paleothermometer. *Paleoceanography and Paleoclimatology*, *33*, 281–301. https://doi.org/10.1002/2017PA003201

Tierney, J. E., Zhu, J., King, J., Malevich, S. B., Hakim, G. J., & Poulsen, C. J. (2020). Glacial cooling and climate sensitivity revisited. *Nature*, *584*(7822), 569–573. https://doi.org/10.1038/s41586-020-2617-x

Turner, S. K., Sexton, P. F., Charles, C. D., & Norris, R. D. (2014). Persistence of carbon release events through the peak of early Eocene global warmth. *Nature Geoscience*, *7*(10), 748–751. https://doi.org/10.1038/ngeo2240

Utescher, T., Bruch, A. A., Erdei, B., Francois, L., Ivanov, D., Jacques, F. M. B., et al. (2014). The coexistence approach—Theoretical background and practical considerations of using plant fossils for climate quantification. *Palaeogeography, Palaeoclimatology, Palaeoecology*, *410*, 58–73. https://doi.org/10.1016/j.palaeo.2014.05.031

von der Heydt, A. S., Dijkstra, H. A., van de Wal, R. S., Caballero, R., Crucifix, M., Foster, G. L., et al. (2016). Lessons on climate sensitivity from past climate changes. *Current Climate Change Reports*, *2*(4), 148–158. https://doi.org/10.1007/s40641-016-0049-3

Von Schuckmann, K., Palmer, M. D., Trenberth, K. E., Cazenave, A., Chambers, D., Champollion, N., et al. (2016). An imperative to monitor Earth's energy imbalance. *Nature Climate Change*, *6*(2), 138–144. https://doi.org/10.1038/nclimate2876

Warny, S., Askin, R. A., Hannah, M. J., Mohr, B. A. R., Raine, J. I., Harwood, D. M., & Florindo, F.; SMS Science Team. (2009). Palynomorphs from a sediment core reveal a sudden remarkably warm Antarctica during the middle Miocene. *Geology*, *37*(10), 955–958. https://doi.org/10.1130/g30139a.1

West, C. K., Greenwood, D. R., & Basinger, J. F. (2015). Was the Arctic Eocene 'rainforest' monsoonal? Estimates of seasonal precipitation from early Eocene megafloras from Ellesmere Island, Nunavut. *Earth and Planetary Science Letters*, *427*, 18–30. https://doi.org/10.1016/j.epsl.2015.06.036

Westerhold, T., Marwan, N., Drury, A. J., Liebrand, D., Agnini, C., Anagnostou, E., et al. (2020). An astronomically dated record of Earth's climate and its predictability over the last 66 million years. *Science*, *369*(6509), 1383–1387. https://doi.org/10.1126/science.aba6853

Willis, M. J., Zheng, W., Durkin, W. J., Pritchard, M. E., Ramage, J. M., Dowdeswell, J. A., et al. (2018). Massive destabilization of an Arctic ice cap. *Earth and Planetary Science Letters*, *502*, 146–155. https://doi.org/10.1016/j.epsl.2018.08.049

Wilson, D. S., Pollard, D., DeConto, R. M., Jamieson, S. S. R., & Luyendyk, B. P. (2013). Initiation of the West Antarctic ice sheet and estimates of total Antarctic ice volume in the earliest Oligocene. *Geophysical Research Letters*, *40*, 4305–4309. https://doi.org/10.1002/grl.50797

Witkowski, C. R., Weijers, J. W. H., Blais, B., Schouten, S., & Damsté, J. S. S. (2018). Molecular fossils from phytoplankton reveal secular P_{CO_2} trend over the Phanerozoic. *Science Advances*, *4*(11), eaat4556. https://doi.org/10.1126/sciadv.aat4556

Wong, T. E., Cui, Y., Royer, D. L., & Keller, K. (2021). A tighter constraint on Earth-system sensitivity from long-term temperature and carbon cycle observations. *Nature Communications*, *12*(1), 3173. https://doi.org/10.1038/s41467-021-23543-9

Wunderling, N., Willeit, M., Donges, J. F., & Winkelmann, R. (2020). Global warming due to loss of large ice masses and Arctic summer sea ice. *Nature Communications*, *11*(1), 5177. https://doi.org/10.1038/s41467-020-18934-3

Zeebe, R. E. (2013). Time-dependent climate sensitivity and the legacy of anthropogenic greenhouse gas emissions. *Proceedings of the National Academy of Sciences of the United States of America*, *110*(34), 13739–13744. https://doi.org/10.1073/pnas.1222843110

Zeebe, R. E., Ridgwell, A., & Zachos, J. C. (2016). Anthropogenic carbon release rate unprecedented during the past 66 million years. *Nature Geoscience*, *9*(4), 325–329. https://doi.org/10.1038/ngeo2681

Zelinka, M. D., Myers, T. A., McCoy, D. T., Po-Chedley, S., Caldwell, P. M., Ceppi, P., et al. (2020). Causes of higher climate sensitivity in CMIP6 models. *Geophysical Research Letters*, *47*, e2019GL085782. https://doi.org/10.1029/2019GL085782

Zhang, Y. G., Henderiks, J., & Liu, X. (2020). Refining the alkenone pCO_2 method II: Towards resolving the physiological parameter '*b*'. *Geochimica et Cosmochimica Acta*, *281*, 118–134. https://doi.org/10.1016/j.gca.2020.05.002

Zhu, J., Poulsen, C. J., & Tierney, J. E. (2019). Simulation of Eocene extreme warmth and high climate sensitivity through cloud feedbacks. *Science Advances*, *5*(9), eaax1874. https://doi.org/10.1126/sciadv.aax1874

References From the Supporting Information

Lauvset, S. K., Key, R. M., Olsen, A., van Heuven, S., Velo, A., Lin, X., et al. (2016). A new global interior ocean mapped climatology: The 1° × 1° GLODAP version 2. *Earth System Science Data*, *8*, 325–340. https://doi.org/10.5194/essd-8-325-2016

Zachos, J. C., Stott, L. D., & Lohmann, K. C. (1994). Evolution of early Cenozoic marine temperatures. *Paleoceanography and Paleoclimatology*, *9*(2), 353–387. https://doi.org/10.1029/93PA03266

Zeebe, R. E., & Tyrrell, T. (2019). History of carbonate ion concentration over the last 100 million years II: Revised calculations and new data. *Geochimica et Cosmochimica Acta*, *257*, 373–392. https://doi.org/10.1016/j.gca.2019.02.041